STRUCTURAL, BIOCHEMICAL AND BIOPHYSICAL STUDIES OF THE BACTERIAL FLAGELLAR SWITCH COMPLEX

A Dissertation
Presented to the Faculty of the Graduate School
of Cornell University
In Partial Fulfillment of the Requirements for the Degree of
Doctor of Philosophy

by
Gabriela Gonzalez-Bonet
May 2010

STRUCTURAL AND BIOCHEMICAL STUDIES OF THE BACTERIAL FLAGELLAR SWITCH COMPLEX

Gabriela Gonzalez-Bonet, Ph. D.

Cornell University 2010

Many bacteria use flagella operated by rotary motors to swim. These complex structures contain more than 25 different proteins that self assemble to generate torque and regulate the sense of flagellar rotation. A key molecular event during chemotaxis is the interaction between the phosphorylated response regulator CheY (CheY-P) and the flagellar switch complex, which serves to switch the direction of flagellar rotation between clockwise and counterclockwise, in to order tumble or swim smoothly, respectively. The flagellar switch complex, composed of FliM, FliG and FliN, is responsible for the changes in the direction of rotation of the flagella, torque generation and flagellar assembly. FliM is the switch complex component that interacts with CheY-P and with the other two components of the switch complex and it is known to be important for flagellar assembly. FliG is known to interact with the motor complexes MotAB, which provide the energy necessary for torque generation. However, the interaction FliG-FliM is not primarily involved in flagellar assembly or torque generation but instead might play a critical role in switching. To understand the mechanism of flagellar switching and its relationship to torque generation and signal amplification, I have cloned, expressed, purified,

characterized and crystallized for the first time a two-component flagellar switch complex FliM/FliG. The structure is in agreement with biochemical and mutational experiments in terms of interaction interface between FliG and FliM. Also, the structure shows an interesting conformation of FliG middle domain that is different to the one previously reported. A FliM dimer is reported and extensive biophysical studies have being performed to try to understand FliG – mediated FliM self-assembly and how relevant it is to switching. Our crystal structure and biochemical studies provide new insights into a more complete model for the molecular mechanism of flagellar motor switching.

BIOGRAPHICAL SKETCH

Gabriela Gonzalez-Bonet was born in San Juan, Puerto Rico on August 14, 1981 to Roberto Gonzalez and Awilda Bonet. She graduated from Cupey Maria Montessori School with high honors in 1999 and was accepted to the University of Puerto Rico (UPR), Rio Piedras campus as part of the "Grupo de los 100" (Best 100 students) of the College of Natural Sciences in the Department of Biology with the goal of pursuing a career in Medicine. After the first semester into her degree she felt in love with her chemistry class and decided to change her major to Chemistry. During her sophomore year she started exploring the world of the basic science research working as an undergraduate research assistant with the guidance of Dr. Fernando Gonzalez. During her junior and senior years she obtained a competitive NIH MARC fellowship that funded her research. During the summer of 2002 she completed a research internship with the Leadership Alliance Program at Cornell University, Ithaca, NY with Dr. George Hess. She then finished her bachelor in science with *Magna Cum Laude* honors in 2003. With the blessing of her parents and brother, Andres, she decided to leave her beloved island to pursue a Ph.D. at Cornell University in the Field of Biochemistry, Molecular and Cell Biology. As a NIH pre-doctoral fellow she pursued her graduate training with Dr. Brian Crane in the Department of Chemistry and Chemical Biology.

Gabriela is married to her soul mate, Daniel. They both are blessed with a son, Diego Sebastian.

A mi mami, papi y hermano por su amor y dedicacion incondicional.

A mi esposo por su apoyo constante.

A mi bebe por ser mi inspiracion y motivacion en todo lo que hago.

ACKNOWLEDGMENTS

I would like to thank my family first and foremost. Thank you mom and dad for all your endless love and support and for teaching me the importance of higher education. Thanks to my little brother Andres, because you always believe in me and because even when you think I am your role model, you are the one I follow. Thank you, Daniel for being always there in good and bad times, for being supportive and making my life easier and more fun. Thanks to my baby Diego, because even when you do not realize this now, you are the motor that drives forward everything I do, and because with your eyes and smile you make me feel like the most important and intelligent person in this world. I also want to acknowledge my advisor Dr. Brian Crane for his patience and mentoring not only in the professional aspects but also family-oriented areas. I want to specially thank my committee members, Dr. Steven Ealick and Dr. Richard Cerione for all your feedback and scientific discussions. Thank you Dr. George Hess for being my very first mentor in Ithaca and for always being there. Joanne Widom, Alexandrine Crane and Sang Young Park, thank you all for being the best lab trainers and passing your wisdom. I cannot forget all my friends back in Puerto Rico, especially Natasha and Elizabeth because you have proofed that distance is not a barrier for friendship. My family in USA: “Boricua” friends at Cornell, especially to my best friend “compadre” Nelson because from day one in Ithaca I knew that I could count on you not only as a friend but also as a

brother; The “Boricua” friends in USA, especially my “compadre” Arnaldo and Naomi, because we are all supporting each other while surviving graduate school; The Crane Lab friends, especially Abiola for making my lab days more fun and interesting and last but not least, The mama friends, especially Harumi for your support and for making the new chapter of motherhood a very fun one. Finally, I want to thank everyone I may have forgotten to mention.

TABLE OF CONTENTS

Biographical Sketch.....iii

Dedication.....iv

Acknowledgements.....v

Table of contents.....vii

List of Figures.....x

List of Tables.....xiii

Chapter 1: Introduction

1.1 Bacterial Chemotaxis as a Signaling Pathway.....1

1.2 Chemotaxis as a two-component system.....2

1.3 The Bacterial Flagellar Motor.....5

1.4 Flagellar Switch Complex.....7

FliM is crucial in the switching mechanism.....8

FliN might be involved in flagellar assembly and export...9

FliG talks to the stator (MotAB) to generate torque.....10

FliM and FliG interaction.....11

Chapter 2: Stable analogs of Phosphono-CheY (CheY-P)......25

2.1 Introduction.....25

2.2 Methods and Materials 28

CheY mutagenesis and phonomethylation.....28

CheY D10KY101W 28

2.3 Preliminary results 29

Chapter 3: Structural and biochemical studies of the Flagellar Switch Complex omponents FliM and FliG 32

3.1 *Introduction*.....32

3.2 Materials and Methods.....33

Protein Preparation 33

Crystallization and Data Collection.....34

Structure Determination and Refinement.....34

Protein mutagenesis and spin-labeling 34

Pulsed-ESR measurements 36

3.3 Results

In-vitro reconstitution of flagellar complexes 37

Crystallization of FliM and FliG complex 41

FliM and FliG complex structure.....42

Electron Spin Resonance experiments

of FliM and FliG.....46

3.4 *Discussion*

FliGm195/FliMm crystal structure.....52

Highly conserved residues are involved in

FliGm195/FliMm interaction.....53

FliG "linker" peptide 55

FliM-FliM self-association.....56

Electron Spin Resonance Studies of the Flagellar

Switch Complex.....57

The Basics 57

Evidence of FliM self-associates using ESR

Spectroscopy.....58

FliG c-terminal re-arrangement 59

Chapter 4: Modeling the flagellar motor switching mechanism...64

4.1 FliM, FliN and FliG location.....64

4.2 Molecular Mechanism of Flagellar Motor Switching.....66

Amplification at the switch level 68

Previous flagellar switch complex models 70

New flagellar switching model.....71

4.4 Conclusion.....74

Appendix A: Bacterial Chemotaxis Studies in Different Models ..77

Flagellar homologues.....77

Non-flagellar homologues 80

Appendix B: The FliN/FliY dilemma 83

Appendix C: *Thermotoga maritime* CheY Deactivation* 93

Introduction 93

Methods and materials 94

Radioactive Dephosphorylation assays

Results and Discussion 95

LIST OF FIGURES

Figure 1.1 Bacterial chemotaxis mechanism 3

Figure 1.2 Behavior of bacterial cells.....4

Figure 1.3 Schematic side view of a H+-driven flagellar motor of Gram-negative bacteria.....5

Figure 1.4 Molecular architecture of the intact flagellar motor in *Borrelia burgdorferi* revealed by Cryo-Electron Tomography 6

Figure 1.5 Multialignment of FliM sequences from various bacterial species 12

Figure 1.6 Multialignment of FliG sequences from various bacterial species.....14

Figure 2.1 Stable CheY phosphoryl analog BeF_3^-.....26

Figure 2.2 Phosphonomethylation of CheY.....27

Figure 2.3 MALDI-TOF linear Mode Spectrum of Phosphono-CheY 29

Figure 3.1 Reaction of methanethiosulfonate spin label with a cysteine-containing protein to produce the nitroxide side chain.....36

Figure 3.2 TMFliM/TMFliG pull down assay.....38

Figure 3.3 Size exclusion chromatography profile for *Thermotoga maritima* $FliM_{1-249}$ and FliGmc 39

Figure 3.4 Size exclusion chromatography profile for *Thermotoga maritima* $FliM_{1-249}$ and FliGm195 40

Figure 3.5 FliM+FliGm195 crystals 41

Figure 3.6 FliM/FliGm195 crystal structure 44

Figure 3.7 Comparison of the FliG middle domain in our structure vs. the one previously published by the Blair lab.....45
Figure 3.8 FliM antiparallel dimer observed in the crystal structure 46
Figure 3.9 Effect of different fragments of wild type FliG on FliM 60.....48
Figure 3.10 Comparison of CheY-BeF3 and CheY-phosphono on FliM oligomerization.....49
Figure 3.11 Effect of CheY, Phosphono CheY and CheY active double mutant on FliM self-association in presence of wild type FliGmc 50
Figure 3.12 Effect of CheY and Phosphono CheY on FliG self-association in presence of wild type FliM.....51
Figure 3.13 Distances between FliM60 and FliG274 and 305.....52
Figure 3.14 Blair's hypothesized small rotation of FliCc agrees with the ESR data..... 60
Figure 4.1 Ultrastructure of the flagellar basal body 65
Figure 4.2 Model I: Assemby of FliMm and FliGm195 based on Park *et al.* model for FliM assembly 69
Figure 4.3 FliM regions of interaction 71
Figure 4.4 Proposed molecular mechanism of CheY-promoted flagellar motor switching.....74
Figure A1 Size Exclusion Chromatography profiles..... 79
Figure A2 DifD and DifG protein purification and crystallization.....81
Figure B1 Structure of FliM reveals homology to the CheC/CheX phosphatase family 84

Figure B2 Domain organization for the CheC/CheX/FliY phosphatase family in *T.maritima, B.subtilis* and *B.anthracis* 85

Figure B3 FliY is annotated as an authentic frameshift mutant 86

Figure B4 $FliY_{FL}$ cloning and mutation..... 87

Figure B5 Size exclusion chromatography profiles of FliY full length and other flagellar switch complex components.....88

Figure B6 Bacillus anthracis has two CheC domains and one FliN domain 89

Figure B7 BaFliY crystal needles and SDS gel showing highly pure and well express protein 90

Figure C1 CheC/CheX/FliY phosphatase family and FliM flagellar motor component..... 94

Figure C2 Activities of *T. maritima* CheC, CheX, and CheD.....97

LIST OF TABLES

Table 3.1 Protein samples cloned, purified and prepared for ESR experiments 35

Table 3.2 Data collection and refinement statistics 42

Table A1 Flagellar Switch Complex full length and fragment components cloned from *Thermotoga maritime* using different expression vectors.....78

Table A2 Flagellar Switch Complex full length and fragment components and non-flagellar homologs cloned from *Bacillus subtilis, Geobacillus stearothermophilus, Bacillus anthracis* and *Myxococcus xanthus* using different expression vectors.....80

Table B1 Summary of re-cloning strategy of BaFliY 90

Table B2 Bacterial species predicted to contain both FliY and FliN..... 91

CHAPTER 1

INTRODUCTION

1.1 Bacterial Chemotaxis as a Signaling Pathway

Living organisms process extracellular information or stimuli via signal transduction pathways. Examples of extracellular stimuli include changes in pH, attractant and repellent chemical concentrations, temperature, light and presence of other organisms. Possible responses include gene expression, division, virulence and active movement towards a favorable environment. Most signal transduction pathways in eukaryotes involve phosphorylation by serine, threonine or tyrosine kinases. In prokaryotes, histidine kinase proteins are central player in signaling events that generate cellular responses. Because histidine kinases are essential in bacterial signal transduction pathways and are completely absent in humans, they are a potential target for anti-microbial drug development [1].

Chemotaxis, a phenomenon by which motile bacterial cells respond to chemical gradients by moving toward a favorable environment, is one of the most studied signal transduction pathways in prokaryotes. This signal transduction pathway manifests remarkable sensitivity, gain and feedback control. Sensitivity is due to the amplification of the signal at the level of the receptor and the flagellar motor. It is important for the cell to generate the right output signal by modulating the direction or speed of flagellar rotation. In some pathogens, motility and chemotaxis are crucial for colonization and infection [2]. Signaling systems that mediate such responses are

of interest, not only in representing a fundamental strategy for intracellular information processing, but also as potential targets for antimicrobial drug development.

1.2 Chemotaxis as a two-component system

Two-component systems often control bacterial gene expression, division, chemotaxis and virulence. The components of the chemotaxis signaling system are the sensor histidine kinase, CheA, and the response regulators, CheY and CheB (Figure 1.1). The chemotaxis mechanism involves the binding of a ligand to the transmembrane methyl-accepting chemoreceptor proteins (MCPs). This binding produces conformational changes in the receptor which then activates the autophosphorylation of the histidine kinase CheA coupled to the receptor through CheW [3]. The gamma phosphoryl group of ATP is transferred to a specific histidine residue of the CheA phosphono transfer domain kinase [4]. CheA-P then transfers the phosphate to a highly conserved aspartate residue of the response regulator CheY [5, 6]. After activation, CheY-P diffuses through the cytoplasm and associates with the flagellar motor inducing change in direction of flagellar rotation (switching). Chemotaxis excitation response involves switching of flagellar rotation between clockwise (CW) and counter-clockwise (CCW).

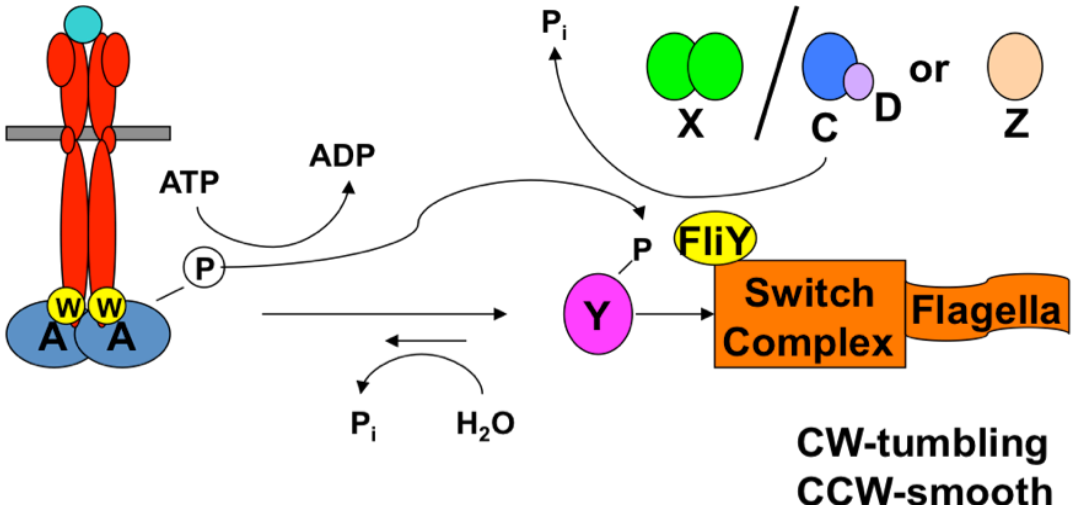

Figure 1.1 Molecular mechanism of bacterial chemotaxis. A ligand binds (teal sphere) to the transmembrane methyl-accepting chemoreceptor proteins (MCPs, red) inducing conformational changes in the receptor that activate the autophosphorylation of CheA. CheA-P then transfers the phosphate to CheY, which then interacts with the flagellar motor to induce changes in the rotation of the flagella. Phosphatases, like CheC/CheX/FliY/CheZ, terminate this signal. The components of the system are label only with the unique letter (e.g. CheX is labeled as X).

The direction of the flagellar rotation determines whether the cell tumbles or swims smoothly [7]. In order to swim smoothly the flagella form a bundle and rotate CCW (Figure 1.2). This bundle is disrupted by the rotation of one flagellum to the opposite direction (CW). This disruption of the bundle produces a tumbling movement and causes the cell to reorient. Then the flagella again form a bundle under CCW movement and thereby smooth swimming re-initiates.

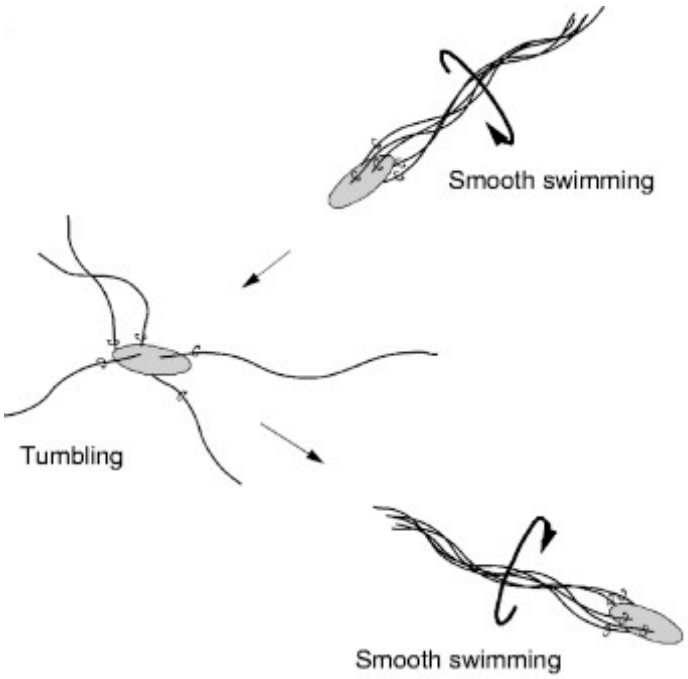

Figure 1.2 Swimming behavior of bacterial cells. In order to swim smoothly the flagella form a bundle and rotate CCW. This bundle is disrupted by the rotation of one flagellum to the opposite direction (CW). This disruption of the bundle is what causes the cell to reorient by producing a tumbling movement. Figure adapted from review [8]

Activated CheY (CheY-P) interacts with the flagellar motor at the location of the flagellar switch complex promoting CW rotation [9]. The switch complex might be intrinsically more stable in conformation CCW under ordinary conditions, only CheY binding to the switch can generate an appreciable probability of CW rotation and so allows the sensory transduction system to effectively moderate motility [10, 11]. This type of mechanism is called stochastic mechanism. The stochastic model asserts, merely, that CheY changes the stabilities of the two rotational states[10].

1.3 The Bacterial Flagellar Motor

The flagellar motor is a molecular machine that converts electrochemical potential energy to mechanical work. More than 50 genes are required for flagellar formation and function. The bacterial flagellum is composed of about 30 different proteins. These protein components localize in the cytoplasm, cytoplasmic membrane, the periplasmic space, outer-membrane and in the extracellular environment (Figure 1.3). These motors are driven by ion-motive force, using either protons or sodium ions.

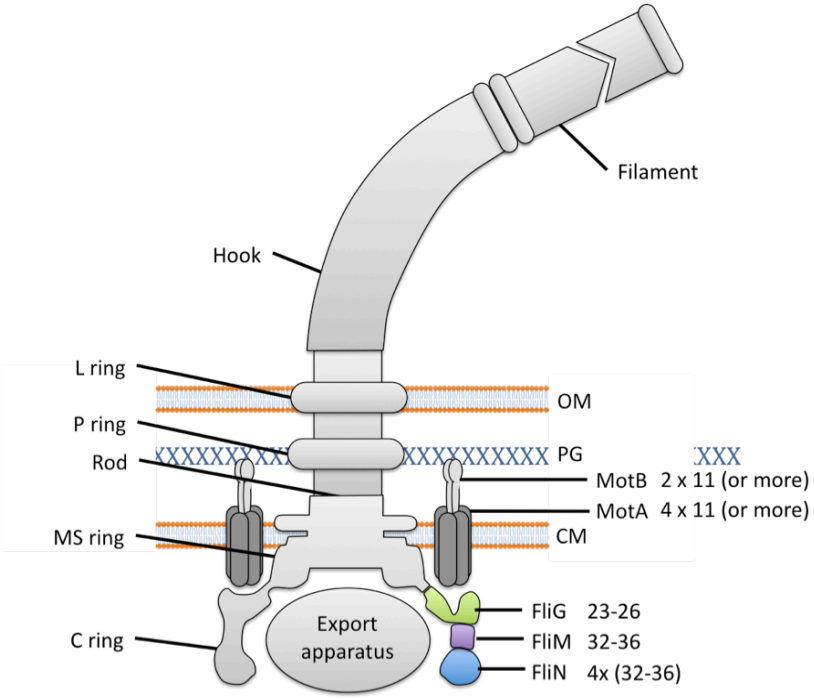

Figure 1.3 Schematic side view of H+-driven flagellar motor of Gram-negative bacteria. The studies in this dissertation focus on the flagellar switch components, FliG, FliM and FliN, which are located at the cytoplasmic ring, better known as the C ring. The figure includes the proposed location and copy number involved in torque generation. OM-outer membrane, PG-peptidoglycan cell wall, CM-cytoplasmic membrane.

Electron microscopy has generated reconstructed detailed images of the flagellar basal body that embeds in the inner membrane and extends into the cytoplasm (Figure 1.4). The MS-ring sits in the membrane and is generated by FliF. The cytoplasmic ring or C-ring extends from the MS-ring to the cytoplasm and it is composed of FliM and FliN. FliG remains partially in the membrane and binds to FliF and also to FliM [12].

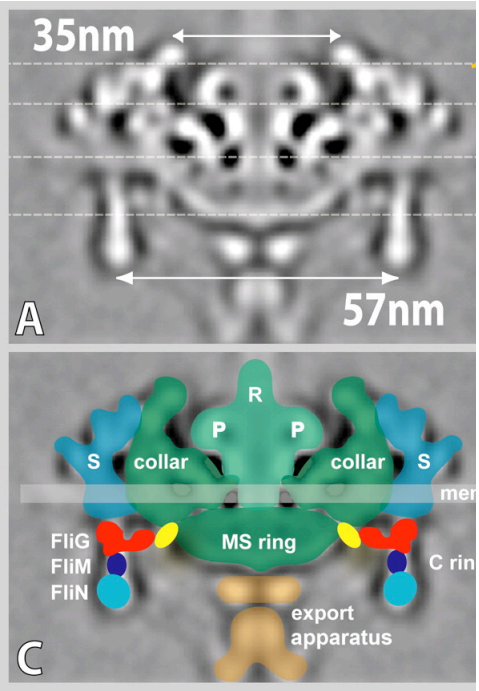

Figure 1.4 Molecular architecture of the intact flagellar motor in *Borrelia burgdorferi* revealed by Cryo-Electron Tomography. A) Central section of flagellar motor oriented perpendicular to the cell axis. C) Model proposed by Liu *et al.* in [13]. The stators (MotAB, teal) can be observed and the location of FliG n-terminal domain is suggested (yellow)

Mutations in the genes that encode FliM, FliG and FliN show abnormal switching, paralysis, or lack of flagella [14] . Several studies have shown that each of these components can generate four different phenotypes: nonflagellated (Fla-), paralyzed (Mot-), switch biased to counterclockwise (Che-[CCW]), and switch biased to clockwise (Che-[CW]). The greatest number of Mot- mutants was in FliG while the greatest number of switch-biased mutant was on FliM, which suggests that FliG is involved mainly in torque generation and flagellar rotation while FliM is mainly involved in switching.

1.4 Flagellar Switch Complex

Genetic (in vivo suppression mutations, yeast-hybrid system), biochemical (in vitro affinity blotting, co-precipitation) and structural (electron microscopy) approaches have shown that FliM, FliN and FliG interact together to form what we call the " flagellar switch complex" [15-20]. This complex is responsible for "switching" or changes in direction of the motor rotation after the binding of CheY-P. However, this is not the only function known. The switch complex is also essential for torque generation and flagellar assembly.

The flagellar switch complex is also known as the C-ring, or cytoplasmic ring because of its shape and location at the cytoplasmic face of the membrane-embedded flagellar basal body [21-23]. The stoichiometry of FliG, FliM, and FliN in the C-ring have been reported to be 26, 34, and ~100 copies, respectively [24-26].

FliM is critical in the switching mechanism

FliM is important for controlling the direction of motor rotation [9, 27]. A null FliM mutant is non-flagellated which suggests that FliM is important and required for flagellar assembly [18]. Mutation experiments suggest the N-terminal two third of FliM is important for switching or CW/CCW bias [27].

Strong evidence points to interactions between cytoplasmic components of the signal transduction pathway (i.e. CheY) and components of the switch complex [6, 11, 15, 27-29]. Previous research has shown that FliM is the component in the flagellar motor that binds directly to the response regulator CheY. We know from genetic and structural studies that CheY binds to the well-conserved FliM N-terminal peptide (LSQXEIDALL) [20, 30-33]. Some studies reveal that the CheY-binding domain on FliM corresponds to the first 15 residues in the N-terminus of FliM including: ten-residue segment deletions [17], crosslinking experiments [31], fluorescence and NMR spectroscopy experiments [32] and x-ray crystallography studies [33]. Nevertheless, deletions experiments of the first 60 residues of FliM revealed coprecipitation with CheY suggesting that multiple domains of FliM are involved in the interaction with the response regulator [34].

With the use of stable phosphate analogs, it has been observed that changes occur in CheY conformation upon phosphorylation in the *Escherichia coli* (*E.coli*) system. The CheY-P and FliM interaction is phosphorylation-dependent since CheY binds stronger to FliM when phosphorylated [30], however is has been seen that CheY still binds to FliM without being phosphorylated. Phosphorylation induces remote

conformational changes in CheY that are responsible for increased affinity with FliM [17, 31, 32]. Early studies suggested that FliM does not directly recognize the phosphoryl group of CheY-P. NMR and x-ray crystallography studies using beryllium fluoride (BeF_3^-) as a phosphate analog show movement of CheY helix-4 (H4) towards the active site [33, 35]. The crystal structure of CheY- BeF_3^- in complex with the first 16 N-terminal residues of FliM shows that the short peptide binds to the H4-β4-H5 face of CheY- BeF_3^-, and this location is actually opposite to the phosphorylation site [33]. It has being previously suggested that H4-β4-H5 face of CheY is an important interaction surface for FliM binding [35, 36]. Another important conformational change involves the position of Tyr 106. In the activated structure, CheY Tyr106 is in a buried conformation. The rotation of Tyr106 into the buried or 'in' position is important because otherwise it would interfere with the binding to the flagellar motor. NMR experiments also confirm the same buried reorientation of Tyr106 in CheY upon activation [35].

FliN may be involved in flagellar assembly and export

FliM not only interacts with CheY but also with FliN, the second component of the flagellar switch complex. FliN has an important role in flagellar assembly and may be implicated in flagellar export [37]. The crystal structure of TMFliN shows a tetramer arrangement similar to that of the HrQB C-terminal domain [38]. The HrQB protein from *P. syrangae* belongs to the secretion apparatus of the type III system used by pathogenic bacteria for the export of virulence factors. FliN

interacts with FliM C-terminal [17, 39, 40] as HrQB interacts with HrQA in the type III system [41]. When FliM is overexpressed in defective FliN mutants, the cells start swarming again[16]. In the same way, when FliN is overexpressed in FliM mutants, the cell also recovers from the defect. These results suggest that FliM and FliN in fact interact with each other. It is believed that FliN and FliM act in a cooperative manner. The null mutant of FliN is non-flagellated and lacks FliM in the cell [42]. The interaction between FliN and FliM is then important for the stability and/or proper folding of FliM [42]. In a FliN/FliM flagellar switch fusion mutant analysis, it was found that these two components act as a unit [39]. Also in electron microscopy experiments by the DeRosier research group show how FliN and FliM associate within the C-ring [21].

FliG talks to the stator (MotAB) to generate torque

The third component of the flagellar switch complex is FliG. The N-terminal domain of FliG is important for flagellar assembly and for proper switching since it is the site of attachment to the MS-ring [16]. If this domain is deleted the mutants show no flagellation [43]. The C-terminal domain is needed for torque generation since this region interacts with the energy generator (stator) of the system. If residues at the C-terminal domain (last 95 residues) are mutated, they show a phenotype where toque generation is abolished [16].

FliG has conserved charged residues clustered on a ridge in the C-terminal domain. It is predicted that this charge-bearing ridge is the region of interaction with MotA (PomA) of the stator. MotA (PomA), with

MotB (PomB), conducts either protons or sodium ions and couples ion flow to produce motor rotation ([12] for review). MotA/MotB are integral membrane proteins surrounding the flagellar basal body[44-48]. This interaction between FliG and MotAB is critical for torque generation. It should be mentioned that the stator is the only region that is static and not labile of the flagellar motor. MotB possesses a peptidoglycan-binding motif in the periplasmic domain that keeping the MotAB accord to the cell membrane [49, 50].

FliM and FliG interaction

A good number of biochemical and mutagenesis experiments have shown that FliG and FliM interact. FliG and FliM are co-isolated when either of the components is tagged with a Glutathione-S-transferase (GST) fusion and purified with glutathione affinity columns [51]. FliG interacts with FliM through the middle domain, as reveled by a yeast hybrid experiment [19]. The Macnab research group showed by affinity blotting a strong interaction between FliM middle domain and FliG [20]. The Blair research group was able to identify more than one region of FliM involved in the interaction with FliG [34]. They identified a highly conserved glycine rich region on FliM. As shown on Figure 1.5, the GGXG motif on FliM is highly conserved. This region is located in the middle domain of FliM and it is very likely to be involved in the interaction between FliG and FliM. In experiments done in the *E. coli* system, a change of a residue in this motif causes reduction in binding to FliG [34]. Previously, Sockett *et al.* also identified mutants in this region that resulted in paralyzed phenotype [27]. However, deletion

Figure 1.5 Multialignment of FliM sequences from various bacterial species. Secondary structural elements are shown above the sequence. Highly conserved residues are shown in black. Residues conserved within either only the first or second of two subfamilies of FliM sequences are shown in red (proteobacteria) and green (Gram-positive bacteria, thermotogae, and spirochetes).

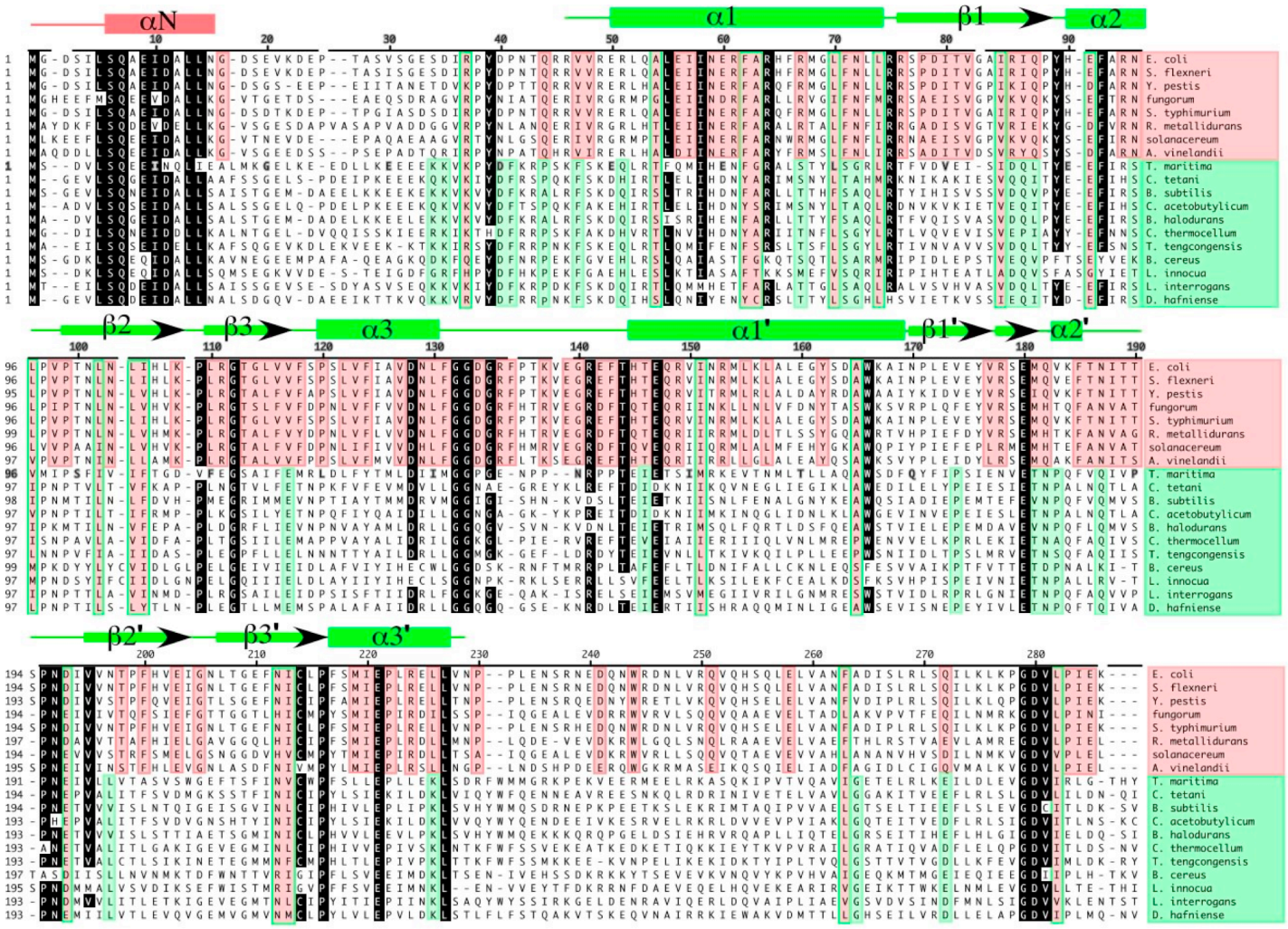
αN
α1
β1
α2
β2
β3
α3
α1'
β1'
α2'
β2'
β3'
α3'
E. coli
S. flexneri
Y. pestis
fungorum
S. typhimurium
R. metallidurans
solanacereum
A. vinelandii
T. maritima
C. tetani
B. subtilis
C. acetobutylicum
B. halodurans
C. thermocellum
T. tengcongensis
B. cereus
L. innocua
L. interrogans
D. hafniense

mutants of the GGXG conserved motif showed no effect in binding with FliG, which suggested that multiple noncontiguous segments of FliM bind to FliG [34].

Also, FliG interacts with FliM through multiple binding sites. FliG has a conserved hydrophobic patch surface in the C-terminal domain opposite to both the charge-bearing ridge and also the highly conserved EHPQR motif on the surface of the middle domain (Figure 1.6). Mutational analysis combined with pull-down assays [52] and two hybrid mutation suppression analysis [53] suggest that these two conserved regions function as sites of interaction with FliM.

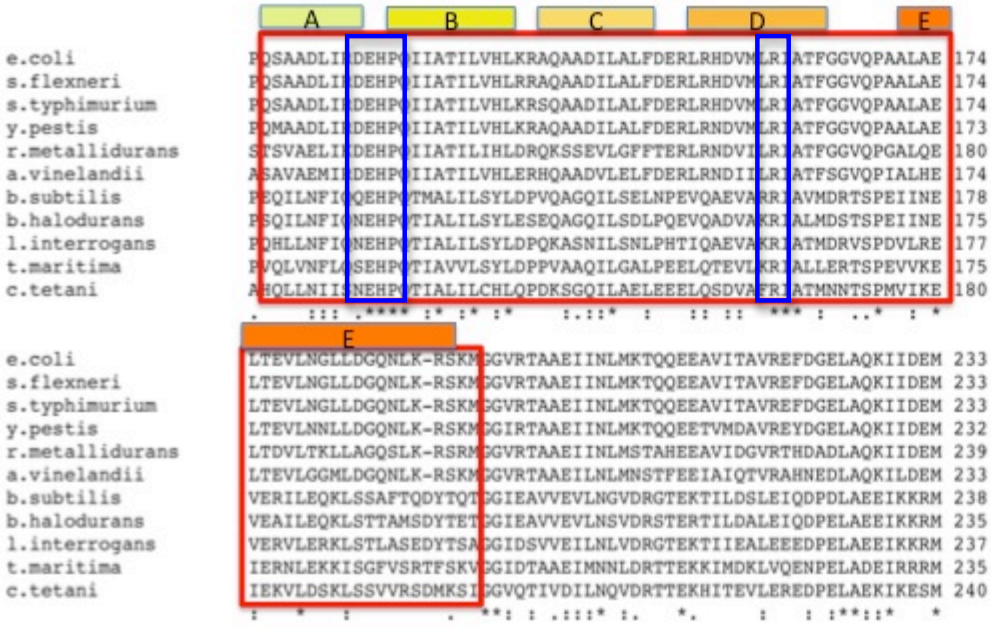

Figure 1.6 Multialignment of FliG sequences from various bacterial species. Red box labels the fragment FliGm195 used in the structural studies described in Chapter 2. Secondary structural elements (e.g. alpha helix) are shown above and are color coded to imitate the color used in Chapter 2 for the structure. Highly conserved residues EHPQ and R (EHPQR motif) are highlighted by a blue box.

By binding to both domains of FliG, FliM could dictate their relative orientation [54]. FliM conformational changes after CheY-P binding could be transmitted to FliG. This interaction between FliM and FliG is critical for switching.

The FliM/FliG ratio in the cytoplasm and flagellar structure seems to be important for proper motility [17] and switching. It has been suggested that conformational changes in FliM induced by the binding of CheY-P could be propagated to the FliG motility domain, triggering the switch between CCW and CW rotation [51]. Unfortunately, this mechanism has yet to be proven. As mentioned previously, the stoichiometry of FliM and FliG is 34 and 26, respectively. Reconstructions from electron cryomicrographs of the rotor revealed that the C-ring has a ~34 fold symmetry and the MS ring shows ~25-fold symmetry [55]. The symmetry of the C-ring matches the number of FliM molecules in the C-ring. The stiochiometry of FliG suggests that it is located between the C-ring and the MS ring with a ratio of 1:1 with the only component of the MS ring, FliF.

Most studies of the flagellar switch complex have been done in *E.coli* and *Salmonella typhimurium*. The best structural information that we currently have on the intact switch complex comes from electron microscopy image re-collection done mainly in *Salmonella*, and more recently in *Borellia burgdorferi*. At the atomic level, the most accurate structural information of the components is from x-ray structural studies of *Thermotoga maritima* components. The crystal structures of individual fragments of *Thermotoga maritima* FliM (16

residues N-terminal peptide, middle domain), FliN (2/3 C-terminal domain) and FliG (middle and C-terminal domain) have been determined [33, 38, 54, 56, 57]. However, in order to elucidate the flagellar switching and torque mechanism and to understand all the biochemical, mutational and physiological data available, more structural information is needed. Especially important, would be structures of complexes of two or more components of the flagellar. In this dissertation, the x-ray crystal structure of a complex between FliM and FliG is presented and an updated structural model for the C-ring is developed to provide new insight into the mechanism of switching.

REFERENCES

1. Wolanin, P.M., P.A. Thomason, and J.B. Stock, *Histidine protein kinases: key signal transducers outside the animal kingdom.* Genome Biol, 2002. **3**(10): p. REVIEWS3013.

2. Butler, S.M. and A. Camilli, *Going against the grain: chemotaxis and infection in Vibrio cholerae.* Nat Rev Microbiol, 2005. **3**(8): p. 611-20.

3. Maddock, J.R. and L. Shapiro, *Polar location of the chemoreceptor complex in the Escherichia coli cell.* Science, 1993. **259**(5102): p. 1717-23.

4. Hess, J.F., R.B. Bourret, and M.I. Simon, *Histidine phosphorylation and phosphoryl group transfer in bacterial chemotaxis.* Nature, 1988. **336**(6195): p. 139-43.

5. Hess, J.F., et al., *Phosphorylation of three proteins in the signaling pathway of bacterial chemotaxis.* Cell, 1988. **53**(1): p. 79-87.

6. Sanders, D.A., et al., *Identification of the site of phosphorylation of the chemotaxis response regulator protein, CheY.* J Biol Chem, 1989. **264**(36): p. 21770-8.

7. Larsen, S.H., et al., *Change in direction of flagellar rotation is the basis of the chemotactic response in Escherichia coli.* Nature, 1974. **249**(452): p. 74-7.

8. Terashima, H., S. Kojima, and M. Homma, *Flagellar motility in bacteria structure and function of flagellar motor.* Int Rev Cell Mol Biol, 2008. **270**: p. 39-85.

9. Welch, M., et al., *Phosphorylation-dependent binding of a signal molecule to the flagellar switch of bacteria.* Proc Natl Acad Sci U S A, 1993. **90**(19): p. 8787-91.

10. Scharf, B.E., et al., *Control of direction of flagellar rotation in bacterial chemotaxis.* Proc Natl Acad Sci U S A, 1998. **95**(1): p. 201-6.

11. Magariyama, Y., S. Yamaguchi, and S. Aizawa, *Genetic and behavioral analysis of flagellar switch mutants of Salmonella typhimurium.* J Bacteriol, 1990. **172**(8): p. 4359-69.

12. Berg, H.C., *The rotary motor of bacterial flagella.* Annu Rev Biochem, 2003. **72**: p. 19-54.

13. Liu, J., et al., *Intact flagellar motor of Borrelia burgdorferi revealed by cryo-electron tomography: evidence for stator ring curvature and rotor/C-ring assembly flexion.* J Bacteriol, 2009. **191**(16): p. 5026-36.

14. Yamaguchi, S., et al., *Subdivision of flagellar genes of Salmonella typhimurium into regions responsible for assembly, rotation, and switching.* J Bacteriol, 1986. **166**(1): p. 187-93.

15. Yamaguchi, S., et al., *Genetic evidence for a switching and energy-transducing complex in the flagellar motor of Salmonella typhimurium.* J Bacteriol, 1986. **168**(3): p. 1172-9.

16. Lloyd, S.A., et al., *Torque generation in the flagellar motor of Escherichia coli: evidence of a direct role for FliG but not for FliM or FliN.* J Bacteriol, 1996. **178**(1): p. 223-31.

17. Toker, A.S., M. Kihara, and R.M. Macnab, *Deletion analysis of the FliM flagellar switch protein of Salmonella typhimurium.* J Bacteriol, 1996. **178**(24): p. 7069-79.

18. Tang, H. and D.F. Blair, *Regulated underexpression of the FliM protein of Escherichia coli and evidence for a location in the flagellar motor distinct from the MotA/MotB torque generators.* J Bacteriol, 1995. **177**(12): p. 3485-95.

19. Marykwas, D.L. and H.C. Berg, *A mutational analysis of the interaction between FliG and FliM, two components of the flagellar motor of Escherichia coli.* J Bacteriol, 1996. **178**(5): p. 1289-94.

20. Toker, A.S. and R.M. Macnab, *Distinct regions of bacterial flagellar switch protein FliM interact with FliG, FliN and CheY.* J Mol Biol, 1997. **273**(3): p. 623-34.

21. Francis, N.R., et al., *Isolation, characterization and structure of bacterial flagellar motors containing the switch complex.* J Mol Biol, 1994. **235**(4): p. 1261-70.

22. Zhao, R., S.C. Schuster, and S. Khan, *Structural effects of mutations in Salmonella typhimurium flagellar switch complex.* J Mol Biol, 1995. **251**(3): p. 400-12.

23. Zhao, R., et al., *FliN is a major structural protein of the C-ring in the Salmonella typhimurium flagellar basal body.* J Mol Biol, 1996. **261**(2): p. 195-208.

24. Francis, N.R., et al., *Localization of the Salmonella typhimurium flagellar switch protein FliG to the cytoplasmic M-ring*

face of the basal body. Proc Natl Acad Sci U S A, 1992. **89**(14): p. 6304-8.

25. Suzuki, H., K. Yonekura, and K. Namba, *Structure of the rotor of the bacterial flagellar motor revealed by electron cryomicroscopy and single-particle image analysis.* J Mol Biol, 2004. **337**(1): p. 105-13.

26. Thomas, D.R., D.G. Morgan, and D.J. DeRosier, *Rotational symmetry of the C ring and a mechanism for the flagellar rotary motor.* Proc Natl Acad Sci U S A, 1999. **96**(18): p. 10134-9.

27. Sockett, H., et al., *Molecular analysis of the flagellar switch protein FliM of Salmonella typhimurium.* J Bacteriol, 1992. **174**(3): p. 793-806.

28. Parkinson, J.S., et al., *Interactions between chemotaxis genes and flagellar genes in Escherichia coli.* J Bacteriol, 1983. **155**(1): p. 265-74.

29. Roman, S.J., et al., *A chemotactic signaling surface on CheY defined by suppressors of flagellar switch mutations.* J Bacteriol, 1992. **174**(19): p. 6247-55.

30. Welch, M., et al., *Effects of phosphorylation, Mg2+, and conformation of the chemotaxis protein CheY on its binding to the flagellar switch protein FliM.* Biochemistry, 1994. **33**(34): p. 10470-6.

31. Bren, A. and M. Eisenbach, *The N terminus of the flagellar switch protein, FliM, is the binding domain for the chemotactic response regulator, CheY.* J Mol Biol, 1998. **278**(3): p. 507-14.

32. McEvoy, M.M., et al., *Identification of the binding interfaces on CheY for two of its targets, the phosphatase CheZ and the flagellar switch protein fliM.* J Mol Biol, 1999. **289**(5): p. 1423-33.

33. Lee, S.Y., et al., *Crystal structure of an activated response regulator bound to its target.* Nat Struct Biol, 2001. **8**(1): p. 52-6.

34. Mathews, M.A., H.L. Tang, and D.F. Blair, *Domain analysis of the FliM protein of Escherichia coli.* J Bacteriol, 1998. **180**(21): p. 5580-90.

35. Cho, H.S., et al., *NMR structure of activated CheY.* J Mol Biol, 2000. **297**(3): p. 543-51.

36. Shukla, D., X.Y. Zhu, and P. Matsumura, *Flagellar motor-switch binding face of CheY and the biochemical basis of suppression by CheY mutants that compensate for motor-switch defects in Escherichia coli.* J Biol Chem, 1998. **273**(37): p. 23993-9.

37. Vogler, A.P., et al., *Salmonella typhimurium mutants defective in flagellar filament regrowth and sequence similarity of FliI to F0F1, vacuolar, and archaebacterial ATPase subunits.* J Bacteriol, 1991. **173**(11): p. 3564-72.

38. Brown, P.N., et al., *Crystal structure of the flagellar rotor protein FliN from Thermotoga maritima.* J Bacteriol, 2005. **187**(8): p. 2890-902.

39. Kihara, M., et al., *Analysis of a FliM-FliN flagellar switch fusion mutant of Salmonella typhimurium.* J Bacteriol, 1996. **178**(15): p. 4582-9.

40. Marykwas, D.L., S.A. Schmidt, and H.C. Berg, *Interacting components of the flagellar motor of Escherichia coli revealed by the two-hybrid system in yeast.* J Mol Biol, 1996. **256**(3): p. 564-76.

41. Fadouloglou, V.E., et al., *Structure of HrcQB-C, a conserved component of the bacterial type III secretion systems.* Proc Natl Acad Sci U S A, 2004. **101**(1): p. 70-5.

42. Tang, H., et al., *Regulated underexpression and overexpression of the FliN protein of Escherichia coli and evidence for an interaction between FliN and FliM in the flagellar motor.* J Bacteriol, 1995. **177**(12): p. 3496-503.

43. Kihara, M., G.U. Miller, and R.M. Macnab, *Deletion analysis of the flagellar switch protein FliG of Salmonella.* J Bacteriol, 2000. **182**(11): p. 3022-8.

44. Chun, S.Y. and J.S. Parkinson, *Bacterial motility: membrane topology of the Escherichia coli MotB protein.* Science, 1988. **239**(4837): p. 276-8.

45. Dean, G.E., et al., *Gene sequence and predicted amino acid sequence of the motA protein, a membrane-associated protein required for flagellar rotation in Escherichia coli.* J Bacteriol, 1984. **159**(3): p. 991-9.

46. Khan, S., M. Dapice, and T.S. Reese, *Effects of mot gene expression on the structure of the flagellar motor.* J Mol Biol, 1988. **202**(3): p. 575-84.

47. Stader, J., et al., *Nucleotide sequence of the Escherichia coli motB gene and site-limited incorporation of its product into the cytoplasmic membrane.* J Bacteriol, 1986. **166**(1): p. 244-52.

48. Zhou, J., R.T. Fazzio, and D.F. Blair, *Membrane topology of the MotA protein of Escherichia coli.* J Mol Biol, 1995. **251**(2): p. 237-42.

49. De Mot, R. and J. Vanderleyden, *The C-terminal sequence conservation between OmpA-related outer membrane proteins and MotB suggests a common function in both gram-positive and gram-negative bacteria, possibly in the interaction of these domains with peptidoglycan.* Mol Microbiol, 1994. **12**(2): p. 333-4.

50. Koebnik, R., *Proposal for a peptidoglycan-associating alpha-helical motif in the C-terminal regions of some bacterial cell-surface proteins.* Mol Microbiol, 1995. **16**(6): p. 1269-70.

51. Tang, H., T.F. Braun, and D.F. Blair, *Motility protein complexes in the bacterial flagellar motor.* J Mol Biol, 1996. **261**(2): p. 209-21.

52. Brown, P.N., et al., *Mutational analysis of the flagellar protein FliG: sites of interaction with FliM and implications for organization of the switch complex.* J Bacteriol, 2007. **189**(2): p. 305-12.

53. Passmore, S.E., R. Meas, and D.L. Marykwas, *Analysis of the FliM/FliG motor protein interaction by two-hybrid mutation suppression analysis.* Microbiology, 2008. **154**(Pt 3): p. 714-24.

54. Brown, P.N., C.P. Hill, and D.F. Blair, *Crystal structure of the middle and C-terminal domains of the flagellar rotor protein FliG.* EMBO J, 2002. **21**(13): p. 3225-34.

55. Thomas, D.R., et al., *The three-dimensional structure of the flagellar rotor from a clockwise-locked mutant of Salmonella enterica serovar Typhimurium.* J Bacteriol, 2006. **188**(20): p. 7039-48.

56. Park, S.Y., et al., *Structure of FliM provides insight into assembly of the switch complex in the bacterial flagella motor.* Proc Natl Acad Sci U S A, 2006. **103**(32): p. 11886-91.

57. Lloyd, S.A., et al., *Structure of the C-terminal domain of FliG, a component of the rotor in the bacterial flagellar motor.* Nature, 1999. **400**(6743): p. 472-5.

CHAPTER 2

STABLE ANALOGS OF PHOSPHO-CHEY (CHEY-P)

2.1 Introduction

The interaction between the chemotaxis kinase, targets, and phosphatases with CheY-P is transient. The rapid turnover of these phosphatases does not permit a stable complex between the response regulator and any partner. The acyl phosphate linkage of CheY-P is extremely labile with a half-life of seconds [1]. Stable CheY phosphoryl analogs are essential for structural characterization. In order to obtain a stable analog of the activated CheY, three different chemical strategies can be used. These strategies involve a constitutively active double mutant of CheY, the use of BeF^{-}_{3}, and synthesis of phosphonomethylated-CheY.

The first approach involves the use of CheY mutants that are active without phosphorylation. The mutant CheY D13KY106W (residues corresponding to *E.coli*), causes both hyperactive (increasing tumbling) phenotype *in vivo* and increase FliM-binding *in vitro* [2-4]. It is suggested by Dyer *et.al.* that these activating mutants do not cause the protein to switch constitutively to the active conformation suggesting that these mutations allows a more facile transformation to the active form [4].

The second approach uses BeF_3^-, which mimics phosphorylation of bacterial response regulators, both structurally and functionally [5]. BeF_3^- forms an tetrahedral geometry of Be with F and O ligands, as occurs with P and its O ligands (Figure C3). Structures of activated

response regulator using BeF_3^- are available [6-8] including complexes with other proteins [9, 10]. The preparation of this phosphoryl analog is sensitive to the presence of NaF^-, $BeCl_2$ and $MgCl_2$.

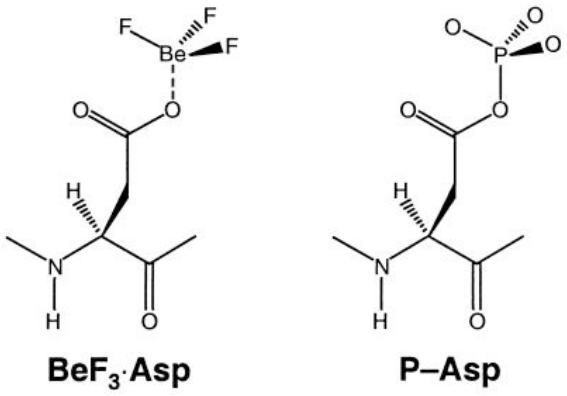

Figure 2.1 Stable CheY phosphoryl analog BeF_3^-. Schematic drawing of the postulated BeF_3^-—Asp complex and its biological counterpart phosphorylated Asp (P-Asp).

CheY-BeF_3^- shows stronger binding to FliM N-terminal domain, higher affinity to CheZ and lower affinity to CheA than CheY, just like CheY-P [5, 11]. An NMR structure of Chey-BeF_3^- reveals structural changes upon activation such as the side chain of Tyr106 restrained in a buried position, and Thr87 forming a hydrogen bond with an active site acceptor [11].

The third approach requires the combination of site directed mutagenesis and chemical modification leading to a stable activated protein, called phosphono-CheY [12, 13] (Figure C4). Details about the synthesis of phosphono-CheY are mentioned in the section of Methods and Materials of this chapter.

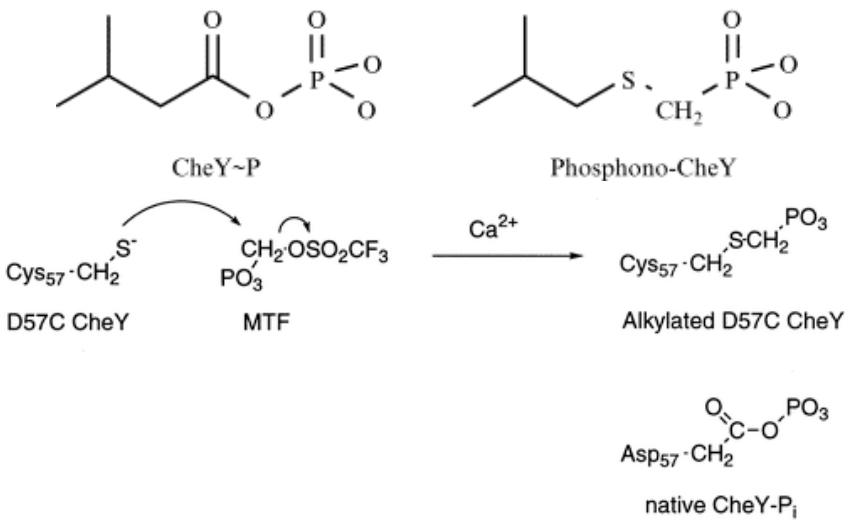

Figure 2.2 Phosphonomethylation of CheY. Comparison of CheY-P to phosphono CheY. Schematic drawing of the phosphonomethylation of D57C CheY.

The phosphono-CheY analog is much more stable than CheY-P and shows the same properties as activated CheY in terms of interaction with FliM and CheZ [13]. Activation by the presence of the phosphonomethyl group also involves propagation of structural changes away from the active site (Asp57 in *E.coli,* Asp54 in *T.maritima*). Opposite to the active double mutant, phosphono-CheY might not distinguish between CW or CCW. Displacement of the Tyr106 from solvent-exposed to a more internal position is also observed for phosphono-CheY. This conformational switch is a hallmark of activation and needed to bind targets.

2.1 Methods and Materials

CheY mutagenesis and phosphonomethylation

The gene encoding *T. maritima* CheY (full-length, residue 1-120) was PCR cloned into the vector pET28a. The *cheY* point mutation of the conserved aspartate D54 into cysteine was introduced by Quickchange mutagenesis and verified by DNA sequencing. After a careful examination of TM CheY sequence and structure, a native cysteine (C81) was found that could complicate modification. Surprisingly, the native cysteine is close enough to the mutant cysteine to form a disulfide bridge. CheY was then subjected to a second site-directed mutagenesis to change C81 into a non-reactive serine (CheY C81S). The CheY double mutant (TM CheY D54C, C81S) was expressed with a 6-His tag in *E. coli* strain BL21 in Terrific Broth with kanamycin selection (25μg/mL). The protein was then purified on Nickel-NTA columns and the His-tags removed by thrombin digestion. The protein was further purified by a Superdex75 sizing column in GF buffer (Tris 50mM pH 7.5, NaCl 150 mM, 10mM DTT) and concentrated by centrifugation. The concentrated CheY double mutant was sent to University of North Carolina at Wilmington, where our collaborator Prof. Christopher Halkides and his graduate student Ryan M. Haas phosphonomethylated the protein.

CheY D10K Y101W

The CheY active mutant was identified in *E.coli.* After sequence alignment of *Thermatoga maritima* and *E.coli cheY,* the residues D13K and P101W were selected for mutagenesis. The aspartate is conserved

in both species (*E.coli* D10) while Phe is an aromatic residue just like Y106. These residues were subjected to mutagenesis following the same protocol mentioned in the previous section.

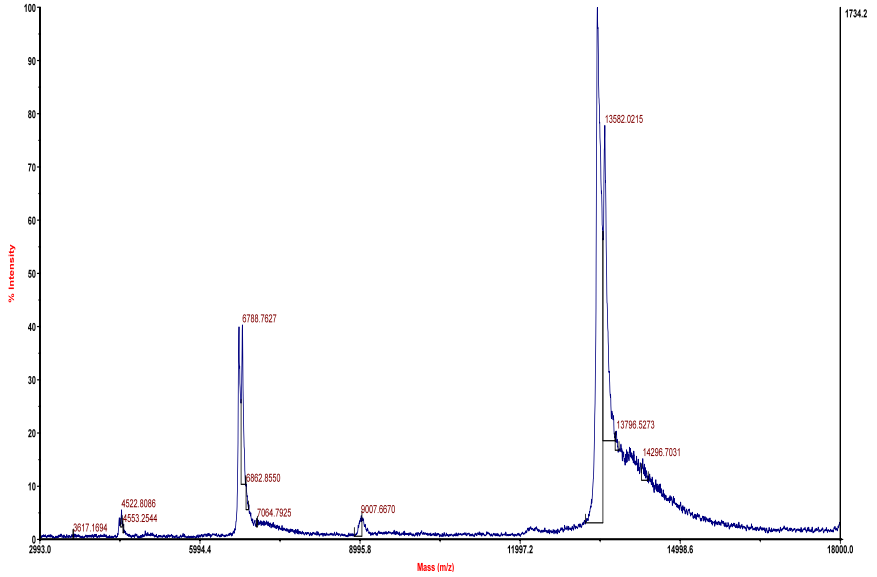

Figure 2.3 MALDI-TOF Linear Mode Spectrum of phosphono-CheY. The highest intensity peak 13582 Da, corresponds to the molecular weight of CheY plus the phosphonomethylation. Also takes in consideration the weight of additional residues after thrombin cleavage after purification.

2.2 Preliminary results

As part of collaboration with the Halkides Research Lab in North Carolina, I performed the mutagenesis of *T.maritima* CheY. The double mutant TMCheY D54C C81S was sent to North Carolina to complete the synthesis of the phosphonomethylated CheY. (See section Methods and Materials for more details). The phophonomethylation was confirmed using MALDI MS (Figure 2.3). In collaboration with Jaya Bhatnagar, the three different CheY analogs mentioned previously were tested for FliM binding (See Chapter 3).

REFERENCES

1. Parkinson, J.S. and E.C. Kofoid, *Communication modules in bacterial signaling proteins.* Annu Rev Genet, 1992. **26**: p. 71-112.
2. Zhu, X., et al., *Tyrosine 106 of CheY plays an important role in chemotaxis signal transduction in Escherichia coli.* J Bacteriol, 1996. **178**(14): p. 4208-15.
3. Scharf, B.E., et al., *Control of direction of flagellar rotation in bacterial chemotaxis.* Proc Natl Acad Sci U S A, 1998. **95**(1): p. 201-6.
4. Dyer, C.M., et al., *Structure of the constitutively active double mutant CheYD13K Y106W alone and in complex with a FliM peptide.* J Mol Biol, 2004. **342**(4): p. 1325-35.
5. Yan, D., et al., *Beryllofluoride mimics phosphorylation of NtrC and other bacterial response regulators.* Proc Natl Acad Sci U S A, 1999. **96**(26): p. 14789-94.
6. Lee, S.Y., et al., *Crystal structure of activated CheY. Comparison with other activated receiver domains.* J Biol Chem, 2001. **276**(19): p. 16425-31.
7. Hastings, C.A., et al., *High-resolution solution structure of the beryllofluoride-activated NtrC receiver domain.* Biochemistry, 2003. **42**(30): p. 9081-90.

8. Gardino, A.K., et al., *The NMR solution structure of BeF(3)(-)-activated Spo0F reveals the conformational switch in a phosphorelay system.* J Mol Biol, 2003. **331**(1): p. 245-54.
9. Lee, S.Y., et al., *Crystal structure of an activated response regulator bound to its target.* Nat Struct Biol, 2001. **8**(1): p. 52-6.
10. Zhao, R., et al., *Structure and catalytic mechanism of the E. coli chemotaxis phosphatase CheZ.* Nat Struct Biol, 2002. **9**(8): p. 570-5.
11. Cho, H.S., et al., *NMR structure of activated CheY.* J Mol Biol, 2000. **297**(3): p. 543-51.
12. Halkides, C.J., et al., *Synthesis and biochemical characterization of an analogue of CheY-phosphate, a signal transduction protein in bacterial chemotaxis.* Biochemistry, 1998. **37**(39): p. 13674-80.
13. Halkides, C.J., et al., *The 1.9 A resolution crystal structure of phosphono-CheY, an analogue of the active form of the response regulator, CheY.* Biochemistry, 2000. **39**(18): p. 5280-6.

CHAPTER 3

STRUCTURAL AND BIOCHEMICAL STUDIES OF THE FLAGELLAR SWITCH COMPLEX COMPONENTS FLIM AND FLIG

3.1 Introduction

Many bacteria use flagella operated by rotary motors to swim. These complex structures contain more than 25 different proteins that self assemble to generate torque and regulate the sense of flagellar rotation. A key molecular event during chemotaxis is the interaction between the phosphorylated response regulator CheY (CheY-P) and the flagellar switch complex, which serves to switch the direction of flagellar rotation between clockwise and counterclockwise, in order to tumble or swim smoothly, respectively. The flagellar switch complex, composed of FliM, FliG and FliN, is responsible for the changes in the direction of rotation of the flagella, torque generation and flagellar assembly. FliM is the switch complex component that interacts with CheY-P and with the other two components of the switch complex and it is known to be important for flagellar assembly. FliG is known to interact with the motor complexes MotAB, which provide the energy necessary for torque generation. However, the interaction FliG-FliM is not primarily involved in flagellar assembly or torque generation but instead might play a critical role in switching. To understand the mechanism of flagellar switching and its relationship to torque generation and signal amplification, I have cloned, expressed, purified, characterized and crystallized for the first time a two-component

flagellar switch complex FliMm/FliGm. The structure is in agreement with biochemical and mutational experiments in terms of interaction interface between FliG and FliM. Also, the structure shows an interesting conformation of FliGm that is different to the one previously reported [1]. Also a FliM dimer is reported and extensive biophysical studies have being performed to try to understand FliG – mediated FliM self-assembly and how relevant it is to switching.

3.2 Materials and Methods

Protein Preparation

Genes encoding *Thermotoga maritima* FliM residues 1-249 (FliMm), the CheY-binding peptide and CheC-like domain, and FliG residues 117-195 (FliGm195), including the middle domain and linker, were PCR cloned into the vector peT28a (Novagen) and expressed with a 6-histidine (His) tag in *E. coli* strain BL21-DE3 (Novagen) in Lysogenic Broth (LB) with kanamycin selection (25μg/ml). The proteins were purified on Nickel-NTA columns, and their His-tags were removed by thrombin digestion. The proteins were combined and further purification on a Superdex200 sizing column (Pharmacia), followed by concentration (Centriprep; Amicon) in GF buffer (50 mM Tris pH7.5, 150 mM NaCl and 4.5 mM DTT). The complex of $FliM_{NM}$ and $FliG_{M}$ was coeluted on the Superdex200 column during a second run.

Crystallization and Data Collection

Multiple initial conditions for growing FliGm195/FliMm complex crystals were found in commercial screening solutions (Hampton). The crystals with the best morphology appeared in a 2ul drop (1:1 mixture of protein in GF buffer and reservoir) from a sealed well under vapor diffusion against a reservoir of 0.1 MES pH 6.5, 10% dioxane and 1.6M ammonium sulfate (Hampton Research). Diffraction data was collected under 100 K nitrogen stream at Cornell High-Energy Synchrotron Source (A1) on a CCD detector (Quantum-210, Area Detector System). The data sets were reduced and scaled using HKL2000 [2].

Structure Determination and Refinement

The FliGm195/FliMm complex structure was determined by molecular replacement with PHASER [3] using as a model the RCSB deposited coordinates PDB codes: 2HP7 (TMFliM) and 1LKV (TMFliG). Several residues of FliGm195 (helices E) were removed from the initial model and rebuilt manually. The final model was refined with the program CNS amidst cycles of manual model building [4].

Protein mutagenesis and spin-labeling

Four residues in the TMFliMm (Glu 60,Asp 79, Asp 121, Ser 167) and four residues in FliGmc (Ser 248, Glu 274, Asp 290, Glu 305) were separately mutated to cysteine (Table 2.1). The cysteine point mutations were introduced by QuickChange mutagenesis and verified

Table 3.1 Protein samples cloned, purified and prepared for ESR experiments. The cysteine mutations were carefully selected in order to be surface exposed for easy labeling.

Protein	Residues	MW (kD)	Labeled?
TMFliMnm	1-249	29.1	No
TMFliMnm 60C	1-249	29.1	Yes
TMFliMnm D121C	1-249	29.1	Yes
TMFliMnm D79C	1-249	29.1	Yes
TMFliMnm S167C	1-249	29.1	Yes
TMFliGmc	104-335	26.3	No
TMFliGmc S248C	104-335	26.3	Yes
TMFliGmc E274C	104-335	26.3	Yes
TMFliGmc D290C	104-335	26.3	Yes
TMFliGmc E305C	104-335	26.3	Yes
TMFliGm169	117-169	5.9	No
TMFliGm195	117-195	8.9	No
TMFliGc	180-335	17.8	No
TMFliGc	195-335	16.1	No
TMFliGc	209-335	14.7	No
TMCheY	1-120	13.2	No
TMCheY BeF-	1-120	13.2	No
TMCheY D10K P101W	1-120	13.2	No
TM phophono-CheY	1-120	13.2	No

by sequencing. Neither protein contains cysteine residues in its native sequence. Proteins were labeled for 4 hours at room temperature and overnight at 4°C with 5–10 mM 1-oxyl-2,2,5,5-tetramethylpyrolinyl-3-methyl)-methanethiosulfonate (MTSSL; Toronto Research, Toronto-Figure 3.1) in gel-filtration buffer (GF) while the His-tagged proteins were bound to nickel–nitrilotriacetic acid agarose beads. The proteins were eluted with GF after 6–12h of incubation with thrombin and then purified using size exclusion chromatography. Incorporation of the label was confirmed by ESR spectroscopy.

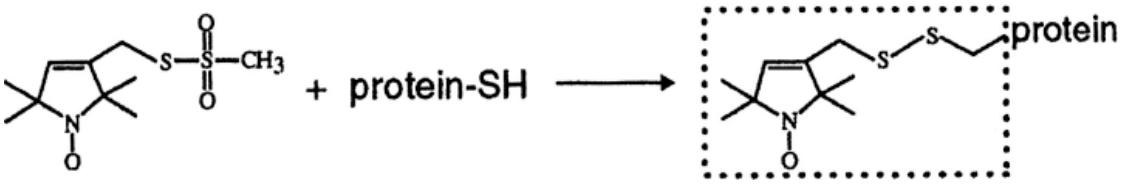

Figure 3.1 Reaction of methanethiosulfonate (MTSSL) spin label with a cysteine-containing protein to produce the nitroxide side chain. In site-directed spin labeling a cysteine is engineered in the desired position and then reacted with MTSSL, which has an unpaired electron.

Pulsed-ESR measurements

For measuring signals from protein complexes, the proteins were mixed together and the sample incubated at room temperature for 30-60 minutes before flash cooling in liquid N_2 for ESR experiments. Protein concentrations were 50 μM each when used for DEER experiments. Concentrations were determined using Bradford Assay.

Pulsed dipolar electron spin resonance spectroscopy (PDS ESR, or PDS for short) yields the distance, *r* between electron spins residing on a molecule of interest. PDS involves measuring magnetic dipolar couplings between two (or more) unpaired electrons. In our case, the spins are nitroxide spin-labels attached specifically to genetically engineered cysteine residues on a protein [5]. Currently, the two most common methods for distance measurements from dipolar spin-couplings are pulsed double electron-electron resonance (DEER or PELDOR) [6] and double-quantum coherence (DQC) [7, 8]. DEER was used during these experiments. DEER requires a less demanding experimental setup and better references the dipolar signal to the subtracted background, which is a desirable feature in the context of this work. Four-pulse DEER experiments were carried out at 17.3 GHz on a specially constructed 2D-FT ESR spectrometer modified to support PDS as described previously [7, 9]. For a review of this method see [10].

3.3 Results

In-vitro reconstitution of flagellar complexes

Crystal structures for *Thermotoga maritima* FliM middle domain (FliMm) and FliG middle and carboxy-terminal domain (FliGmc) have being published previously by the Crane and Blair labs respectively [1, 11]. The first attempt to crystallize a reconstituted complex employed exactly the same fragments used by these groups for crystallization of the individual components. The complex is well behaved in solution. Pull-down assays and size exclusion chromatography data suggest a

tight interaction between these two fragments of FliM and FliG (Figures 3.2 and 3.3). Crystallization of this complex failed despite several attempts using a large range of precipitant, buffers and additives. Other switch complex reconstituted systems in different bacterial species are reported in Appendix A.

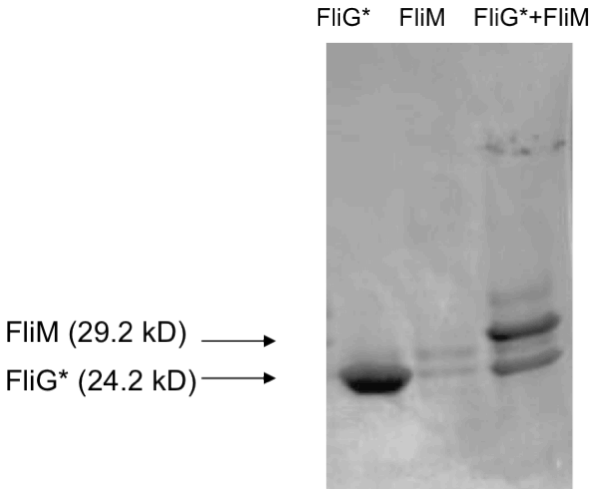

Figure 3.2 TMFliM/TMFliG pull down assay. These experiments were performed using his-tagged labeled FliGmc and $FliM_{1-249}$. The first lane is a control of his-tagged FliG* bound to the Nickel resin, while in the second lane containing only FliM, which lacks a his-tag. In the last lane, an interaction between FliM and FliG* is observed, as FliG* is able to "pull-down" unlabeled FliM.

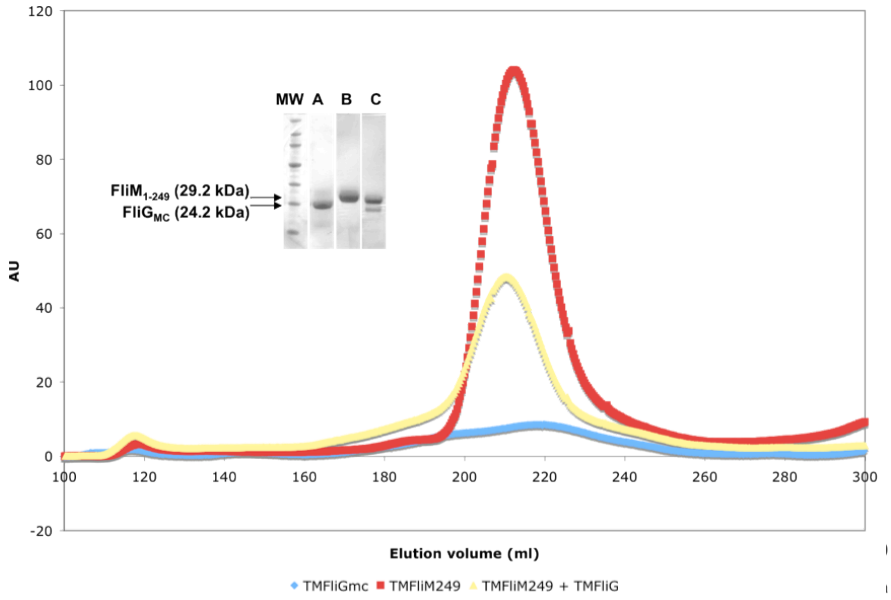

Figure 3.3 Size exclusion chromatography profile for *Thermotoga maritima* FliM$_{1-249}$ and FliGmc. The blue curve corresponds to FliG profile while the red one corresponds to FliM. When FliM and FliG are co-eluted using size exclusion chromatography, a shift towards a higher molecular weight that corresponds to the complex can be observed (yellow curve). One sample corresponding to each peak was run in a SDS-page gel to confirm quality and purity of the proteins and presence of the complex (laneC).

In a new approach to crystallize the complex, FliG middle domain was cloned according to the secondary structural elements and the tertiary structure published by the Blair group [1]. The first two of residues were eliminated because of apparent instability based on the lack of electron density in Blair's maps. The fragment was truncated in two different regions creating two different FliM middle domain fragments. The first clone was truncated at residue 169 (FliGm169), fragment considered by the Blair lab just as the middle domain, while the second clone was truncated at residue 195 (FliGm195) in order to include the long extended linker reported in the

same study. With size exclusion chromatography to reconstitute and characterize the complexes, it was determined that the best behaved system was FliMnm co-eluted with FliMGm195. As it is observed in Figure 3.4, the peak corresponding to the complex shows a shift toward a higher molecular weight. Samples of this peak were run on a SDS gel to prove that in fact it corresponds to the complex. From the SDS gel it is evident that FliGm195 shows two bands, the smaller probably corresponding to the loss of the linker by proteolysis. Such aspects would correspond to fragment FliGm169 because it runs at similar molecular weight on SDS-PAGE compared to this smaller FliGm fragment, which was cloned for comparison (data not shown).

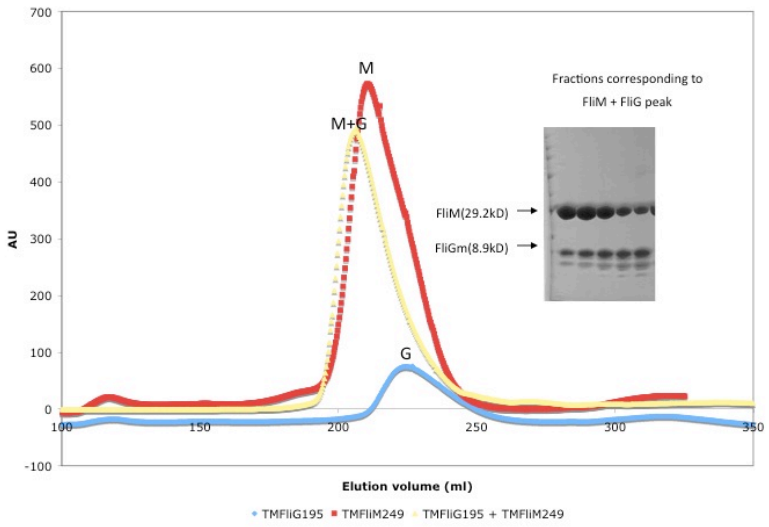

Figure 3.4 Size exclusion chromatography profile for *Thermotoga maritima* FliM$_{1-249}$ and FliGm195. The blue curve corresponds to FliG profile while the red one corresponds to FliM. When FliM and FliG are co-eluted using size exclusion chromatography, a shift towards a higher molecular weight corresponding to the complex is observed (yellow curve). The samples corresponding to the peak corresponding to complex were run in a SDS gel to confirm quality and presence of the complex. Two bands are observed for FliG, one that corresponds to minor proteolytic degradation.

Crystallization of the FliM and FliG complex

Crystallization screens using the re-constituted complex FliMnm/FliGm195 produced crystals in several conditions. Crystals shown in Figure 3.5A were the easiest to reproduce. They appeared in about 3 days using the hanging-drop technique at room temperature and 0.1 M MES pH 6.5, 10% dioxane and 1.6M ammonium sulfate as the reservoir solution. To confirm that these crystals corresponded to the complex and not to an individual component, several crystals were run on a SDS gel (Figure 3.5B) and the band corresponding to the right molecular weight of FliGm195 was sent for mass spectrometry analysis. Two FliGm195 fragments, 158-175 and 182-195, were identified and confirmed from in-gel Glu-C digest and nano LC-MS/MS analysis of the protein band (data not shown). These two fragments correspond to the last 1/3 of FliG middle domain and the linker. At this stage, we were confident that these crystals corresponded to FliGm195/FliMm complex.

Figure 3.5 FliM+FliGm195 crystals. A) Crystals grew in clusters that had to be carefully broken before collecting data. B) Lane 1 is a control of the purified complex in solution while lane 2 corresponds to the crystals fished out from the crystallization drop, rinsed and dissolved in loading buffer. This gel confirms the crystals are of the complex.

FliM and FliG complex structure

The structure of *Thermotoga maritima* FliM middle (FliMm) domain and FliG middle domain (FliGm195) as a complex was determined at 3.5 Å by molecular replacement using the available coordinates for FliM middle domain (FliMm, residues 46-228) and FliG middle and carboxy-terminal domains (FliGmc, residues117-195) (Figure 3.6). Among the 1-249 residues of the expressed FliM protein, the N-terminal 45 residues and the C-terminal 11 residues electron density are absent. Because of the absence of the N-terminal domain, this component will be referred to as FliMm (FliM middle domain) from now on. It is very likely that these regions are disordered in the absence of CheY and/or another flagellar component.

Table 3.2 Data collection and refinement statistics

Parameter	Statistics
Resolution (Å)	15-3.5
Highest resolution shell (Å)	3.5
Observed reflections	14233
Unique reflections	11126
Completeness (%)	78.2
Rwork/Rfree	0.2930/0.3180
Space Group	P3(2)21
Cell Dimensions	91.39, 91.39, 226.52, 90.00, 90.00, 120.00

The structure of FliMm resembles the structure published previously by Park *et al.* [11]. In general, three α-helices (α1-α3) and three β-strands (β1-β3) duplicate to form a pseudo-symmetric α/β/α three-layered sandwich. The six β-strands are antiparallel. A 2-fold symmetry axis perpendicular to the central β-sheet relating the two halves of the protein can be observed.

In the case of FliGm195, we observe electron density corresponding to residues 117-195. This small fragment is composed of five helices (A-E) arranged in a right-handed super-helix. There is a striking difference between the FliGm195 in the complex crystal structure vs. the one published by the Blair lab attached to the C-terminal domain (FliGmc). As Figure 3.7, FliGmc shows an extended alpha helix (E) connecting the middle and the C-terminal domains. In the case of FliGm195 the helix E is packed towards the rest of the compact helical domain hypothetically placing the C-terminal domain in a very different orientation compared with the FliGmc structure.

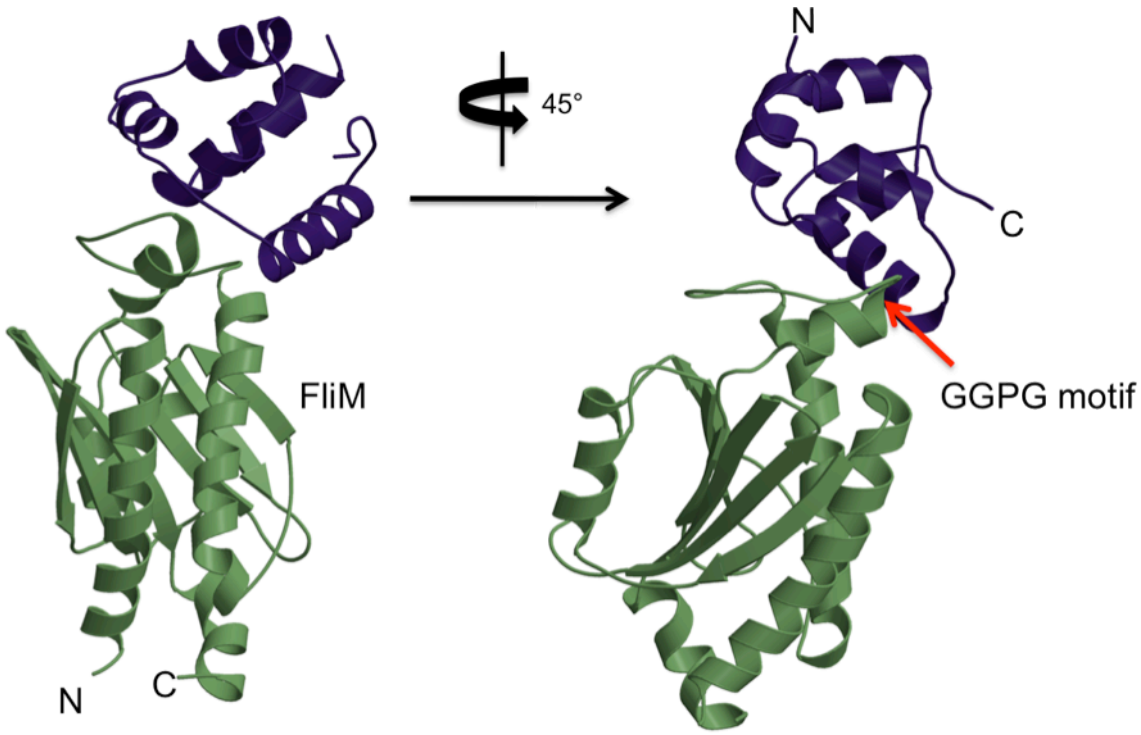

Figure 3.6 FliM/FliGm195 crystal structure. The structure reveals a direct interaction of FliG and FliM through highly conserved residues, including the GGPG motif on FliM α3-α1' loop. C stands for C-terminal while N stands for N-terminal. In the case of FliG the N-terminal domain interacts with the MS ring while the C-terminal domain interacts with the stator MotAB. FliM both N and C-terminal domains are facing in opposite directions to the region of interaction with FliG. The FliM N-terminal domain is known to interact with CheY-P while the C-terminal domain interacts with FliN.

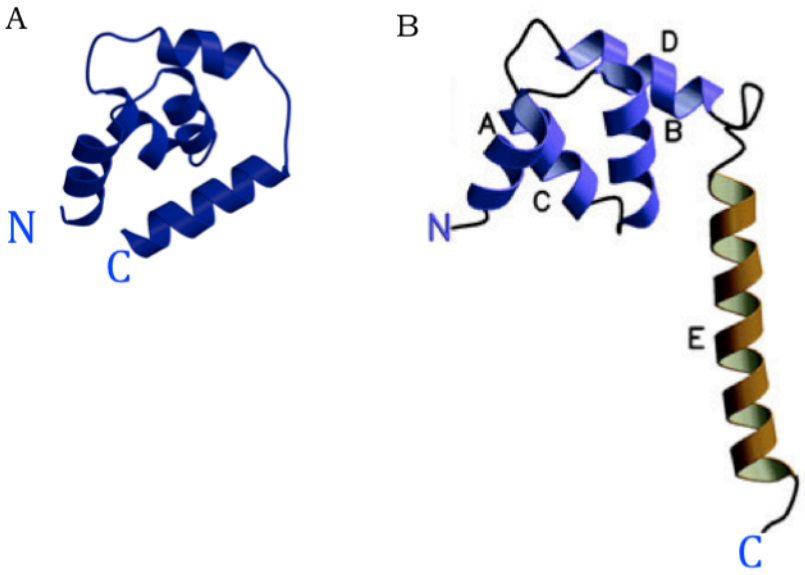

Figure 3.7 Comparison of the FliG middle domain in our structure vs. the one previously published by the Blair lab. A) In our structure, FliG middle domain tertiary structure shows the linker (E) interacting with the core while in B) The linker helix (E) is extended and solvent exposed.

Within the asymmetric unit cell, we find two FliMm molecules and two FliGm195 molecules, with each FliMm binding one FliGm195. The site of interaction in FliM corresponds to the loop between α3 and α1' where the highly conserved GGXG motif is located (Figure 1.5). In the case of FliGm195 the site of interaction includes the highly conserved residues EHPQ between helices A and B (Figure 1.6). The two FliM molecules form an antiparallel dimer with two-fold symmetry (Figure 3.8). The interaction interface in this dimer involves the long helices (∝1 and ∝1') of each molecule. This interaction causes the FliGm195 molecules to be located at opposite sides of the FliM dimer.

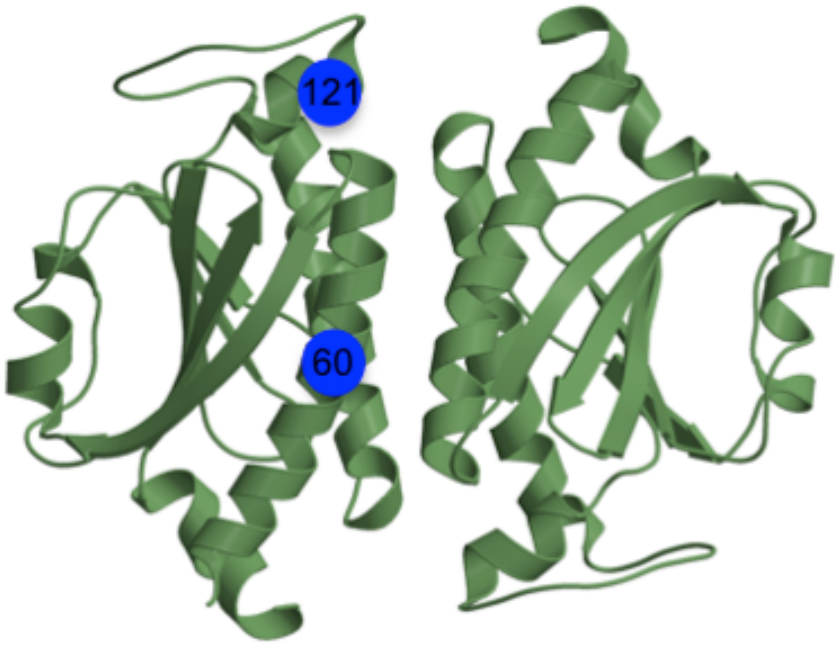

Figure 3.8 FliM antiparallel dimer observed in the crystal structure. The interface involves ∝1 and ∝1'. The loops where the motif GGXG is located are found in opposite directions. The blue spheres correspond to the spin labeled sites used during the ESR experiments. ESR results suggest the presence of a similar dimer in solution.

Electron Spin Resonance experiments of FliM and FliG

As mentioned previously, the reported crystal structure includes FliM middle domain in complex with FliG middle domain. However it would be very interesting to have information on the location of FliG C-terminal domain in order to have a more complete picture of the flagellar switch complex. One technique that is very useful for

mapping domain positions is Pulsed-dipolar electron spin resonance spectroscopy in concert with site-directed spin labeling.

Pulsed dipolar electron spin resonance spectroscopy is a powerful technique for obtaining long-range distance constraints in protein complexes when combining the technique with double spin labeling. The long-distance constraints can be delivered in a distance range of 10 to 80 Å. Information about spin-spin separation distance can be obtained by measuring the dipolar interaction between two spins placed within the protein complex [12] ([10] is a good review of ESR technique). The ESR distance measurements are based on determining the magnitude of the static dipole-dipole couplings between the spins of unpaired electrons of the NO groups of the nitroxides.

With the collaboration of Jaya Bhatnagar of the Crane group we were able to obtain very useful information regarding the interactions between FliM and FliG, FliM and FliM and how different phosphate analogs affect assembly state. Interestingly, we found that both middle and C-terminal domains of FliG are required for FliM oligomerization (Figure 3.9). When either FliGm195 or FliGc was used the signal amplitude stayed the same as the spin labeled FliM alone. Spin labeled FliM itself does not give dipolar signal because it is predominantly a monomer in solution. The oligomerization observed in these experiments indicates FliM dimerization.

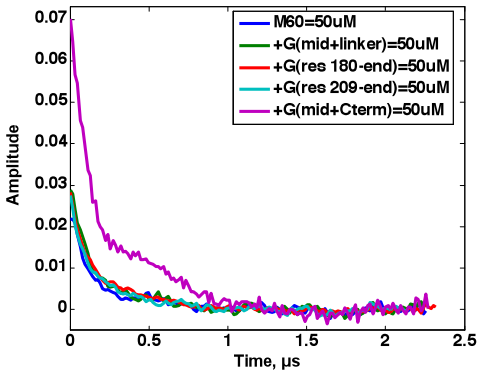

Figure 3.9 Effect of different fragments of wild type FliG on FliM 60. Spin-labeled FliM at residue 60 oligomerize in the presence of FliG middle and c-terminal domain protein fragment (purple curve). The signal in this case increases, suggesting close spin interaction. FliG middle domain (green curve) or the different fragments of FliG C-terminal domain (red and teal curves) alone do not have the same effect. No signal is observed meaning that there is no dipolar interaction between two labeled FliM molecules.

In Figure 3.10a, we can observe CheY-BeF_3^- behaving just like CheY wild type. They both increase FliM signal to the same magnitude, suggesting that FliM oligomerization is formed in the presence of even WT CheY. We see two different oligomer species being produced, one at short distance and one at long distance that are not present in the absence of CheY. Using the same conditions, FliM oligomer population increases even more when phosphono-CheY is present (Figure 3.10b). The double activated mutant (CheY D10K F101W) was also tested (data not shown) but the signal was just like CheY wild type and CheY-BeF_3^-.

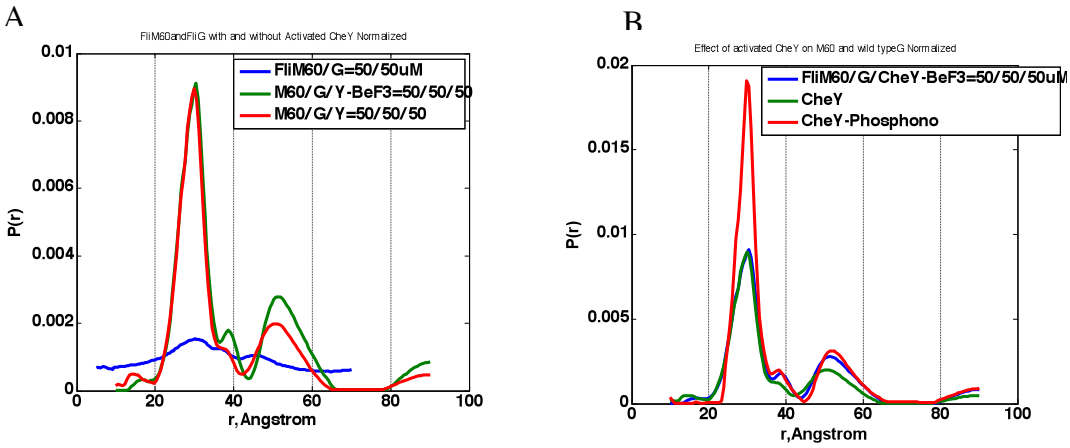

Figure 3.10 Comparison of CheY-BeF3 and CheY-phosphono on FliM oligomerization.

When spin labeled FliM is in the presence of wild type FliG and CheY or phosphono-CheY (a stable phosphate analog, see Chapter 2) the change in the dipolar amplitude varies depending on the position of the spin label (Figure 3.11). In the case of FliM167C, the addition of CheY and phosphono-CheY reduces the dipolar amplitude. We see two different oligomer species, one at short distance and one at long distance, even in the absence of CheY. Inactivated CheY (WT CheY) produces more of the species at the shortest distance compared with phosphono-CheY. For the FliM labeled at residue 121, the addition of CheY WT increases the signal amplitude slightly, while phosphono-CheY increases it to a greater degree. In this case, we see only one main oligomeric species at long distance. In the case of FliM labeled at

residue 60, in the absence of CheY we do not see any signal or presence of a FliM-FliM oligomer. If the inactive CheY is added, the dipolar signal increases, indicating co-localization of the spins and hence oligomerization. Phosphono-CheY increases the signal drastically, increasing the population of oligomer species that gives short distance between spins.

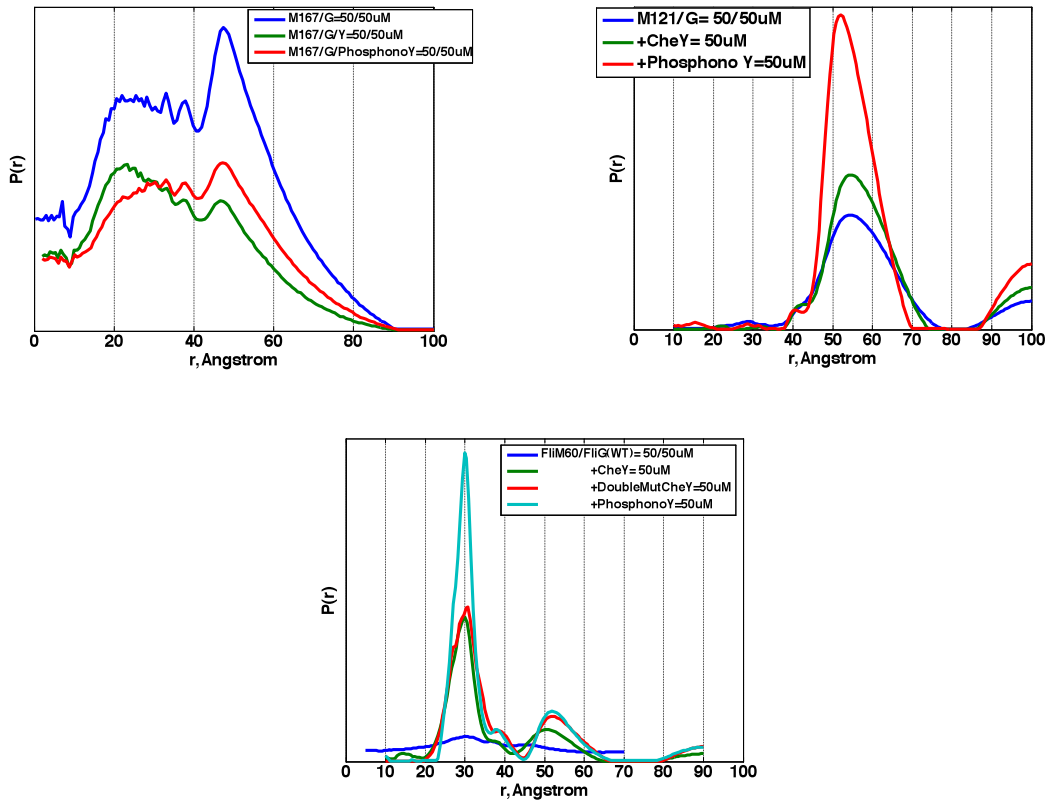

Figure 3.11 Effect of CheY, Phosphono CheY and CheY active double mutant on FliM self-association in presence of WT FliGmc. FliM labeled at the residues 60, 121 and 167 was used during these experiments.

Interesting results were also observed when labeled FliG was tested in the presence of wild type FliM and after addition of inactive CheY or phosphono-CheY (Figure 3.12). The experiments show very broad distributions. When the spin label is at FliGmc residue 305, the signal amplitude increases when phosphono-CheY is present. On the other hand, when FliGmc is labeled at residue 274, the presence of phosphono-CheY decreases the signal amplitude. In both cases even in the absence of CheY, FliG oligomerization is observed.

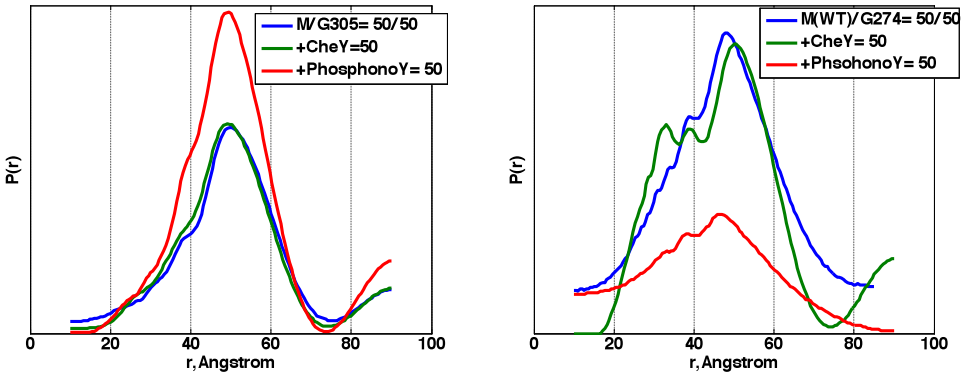

Figure 3.12 Effect of CheY and Phosphono CheY on FliG self-association in presence of wild type FliM. FliGmc spin-labeled at residues 274 and 305 were used.

Experiments with labeled FliM and FliG were performed with the intention to calculate distances between FliM middle domain and FliG c-terminal domain that is not present in the crystal structure. In Figure 3.13 in both experiments we observe only an additive effect, meaning that in both cases, the distance distributions reflect only the

FliG-FliG interactions and FliM-FliM interactions. Additional FliG-FLiM interactions cannot easily be resolved.

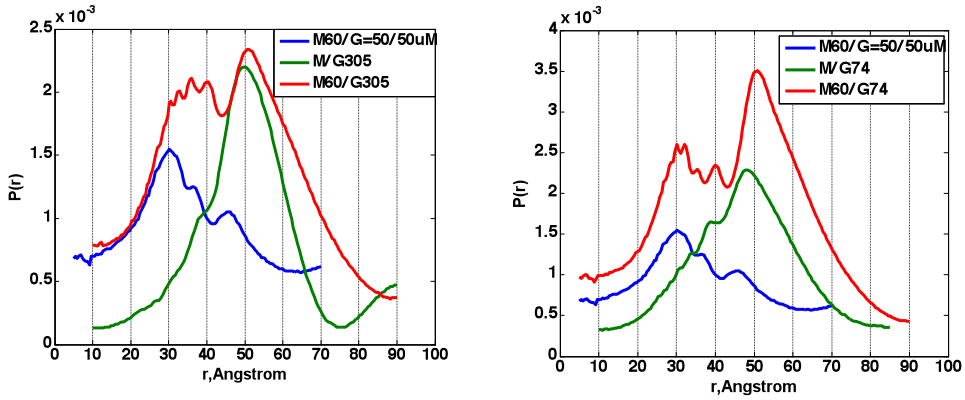

Figure 3.13 Distances between FliM60 and FliG274 and 305

3.4 Discussion

FliGm195/FliMm crystal structure

In this chapter we are reporting for the first time the structure of a complex of switch components. This crystal structure provides much information about the FliM and FliG interaction, the main players of the flagellar switch mechanism. The structure of FliM is quite similar to the one previously reported. The absence of the N-terminal domain of FliM is not a surprise since it is known to be disordered in the context of soluble FliM [11]. In this case, proteolysis is not suspected based on substantial space in the electron density map within the unit cell. Based on the characterization of the complex in solution it seems like FliGm195 gets proteolized and it is very likely that the linker is being cleaved. Fortunately, we were able to obtain the complete FliMm195.

The structure reported is at 3.5 Å resolution. Even though the resolution is not ideal, surprisingly, the electron density is quite good and molecular replacement worked pretty well. There was a great deal of effort to improve the quality of these crystals in order to obtain higher resolution. However, no data set better than 3.5 Å was able to be collected. The diffraction pattern showed anisotropy. Diffraction anisotropy is evidenced as a directional dependence in diffraction quality. These crystals diffracted to higher resolution in the horizontal direction than in the vertical direction. Diffraction anisotropy is commonly observed in protein crystallography, ranging from moderate to severe. It is attributed to whole-body anisotropic vibration of unit cells, for example crystal packing interactions being more uniform in one direction than another. This inherit characteristic of the crystals affected the R-factors but it did not hender the completeness of the crystal structure.

Highly conserved residues are involved in FliGm195/FliMm interaction

During isolation of *fliM* mutations that suppress interaction-disrupting *fliG* mutations [13] it was found that they are located in middle third of *fliM*, more specifically in the region close to the GGXG motif. Our structure shows FliGm195 bound to FliM through this motif. As mentioned in the previous chapter, this motif is highly conserved among several bacterial species (Figure 1.5). This glycine rich region is located in the loop α3-α1' and looks like a linker that

connects the pseudosymmetric halves of FliMm. In the electron maps, the density of this region is weak indicating some mobility of this loop.

The Blair and Marykwas labs have confirmed two regions in FliG that interact with FliM using binding studies with pull down assays and two-hybrid mutation suppression analysis, respectively [13, 14]. One region is located in the middle domain in a highly conserved EHPQR motif (Figure 1.6). This motif is polar and also surface exposed, an ideal location to interact with another component. This motif is present in our FliGm195 fragment and it is in close contact with the GGXG motif of FliM (Figure 3.6). The second binding site on FliG is located at a hydrophobic patch. The residues in this area have conserved hydrophobic properties.

FliG middle domain EHPQR is considered the high affinity-binding site while the hydrophobic region is considered the lower affinity-binding site [13]. Our structural studies include the high affinity-binding site. This suggests that failure during the crystallization of FliM with the middle and c-terminal domain of FliG might be caused by a labile interaction between FliM and the C-terminal domain even when using the same crystallization conditions as of FliMm/FliGm195 complex.

Most FliM mutations identified using the two-hybrid interaction assay also affect switching bias and/or switching frequency. In addition, if a large residue is introduced in any of these two regions during the binding experiements, flagellar assembly or CW/CCW bias is affected. These observations imply that the interaction between FliM and FliG is crucial for flagellar assembly and switching. A model

suggesting how FliG and FliM are involved during switching is explained in detail in the next chapter.

FliG "linker" peptide

The Blair lab determined the crystal structure of FliG middle and C-terminal domain in *Thermotoga maritima* [1]. The coordinates corresponding for the middle domain and the linker were used to solve our structure. The main difference between these two structures is the location of the FliG peptide that links the middle with the C-terminal domain. This linker with extended secondary structure is expected to be fairly flexible based on the presence of two consecutive highly conserved Gly residues between the linker and the c-terminal domain (not included in our FliGm195 fragment).

In the Blair structure this peptide is shown as an extended, rigid and completely solvent exposed α-helix. However this conformation is likely to be a crystallization artifact since it is stabilized by contacts with other FliG molecules in the unit cell. With the high number of hydrophobic residues (>30%), the likelihood that this peptide will be stable completely solvent exposed is low. This does not rule out that this linker can never be in this conformation, since it might be very flexible in solution.

In our structure this linker is in a collapsed conformation making contacts with the FliGm core predicting the location of FliG c-terminal domain to be located at a very different place compared to Blair's structure. These two conformations might be crucial for switching and the change in location or contacts of FliG c-terminal

domain might be responsible of transmitting the signal from FliM to the stators (MotAB) in order to generate torque. Mutations at the beginning of the linker show an extreme clockwise bias mutation [15]. In mutational studies, it was found that out of 26 CW-biased mutations, about half lay between positions 165-195 (linker) [16]. The implications of all these findings in addition with our structural data will be discussed in the next chapter.

FliM-FliM self-association

Not only the interaction between FliM/FliG and FliM/FliN has being studied, but also self-association is a concept of a lot of interest in order to elucidate the switching mechanism [17, 18]. Self-association has being observed between FliG/FliG, FliN/FliN and FliM/FliM during co-precipitation and co-isolation assays [18]. FliM self-association was suggested during deletion analysis where the FliM mutant phenotype was able to incorporate into the flagellar C-ring by probably interacting with WT FliM [19]. The C-terminal domain might be important not only to interact with FliN but also for oligomerization. The N-terminal 50 residues are important for switching but not essential for interaction with FliN or other FliM molecules.

Our structure reveals a FliM dimer that has 2-fold symmetry. This dimer is antiparallel, positioning the FliGm195 in opposite extremes. We do not have enough data to explain the relevance of this dimer and thus it could be a product of crystallization (read next section for more information). Park *et al.* studies suggested self-association of FliM units forming a chain mediated by $\alpha 1$ and $\alpha 2'$ [11].

This data reveals a parallel interaction between opposite faces. A previous model for C-ring assembly was proposed based on cross-linking data, functional analyses, and inter-subunit spacing within the C-ring. In the next chapter, I will present a new model based on FliM assembly in the C-ring with the addition of the FliGm195 and a hypothesized location for the FliG C-terminal domain.

Electron Spin Resonance Studies of the Flagellar Switch Complex

The Basics

ESR has many advantages compared to other techniques. Compared to x-ray crystallography and NMR, ESR requires small amounts of protein, there is no need for crystals, there is no concern about long-term protein stability at high concentration and large biomolecule or complex systems can be studied. Compared to FRET, the ESR label is smaller and only requires one type of probe, usually a nitroxide derivative. Also ESR provides accurate distances between spins.

Applications of the technique had a drastic improvement after the development of site directed spin labeling. This is a convenient method to attach ESR probes to cysteine residues on proteins [5, 20]. This label must reside in the surface of the protein in order to increase the likelihood of interaction between the spin label and the cysteine residue. All cysteine residues introduced to FliM and FliG were carefully selected to be surface exposed and in a position that is known not to be absolutely crucial for protein-protein interaction since we do not want to destroy FliM/FliG binding.

Evidence of FliM self-association using ESR spectroscopy

As mentioned previously, FliM-FliM self associates in the c-ring. This self-association is very likely to be crucial for switching. FliM might be in two different association states distinguishing the different CW and CCW CheY interaction modes. Our ESR studies reveal that FliM oligomerize only when both FliG domains, middle and c-terminal domains, are present (Figure 3.9). We know from the crystal structure that FliG middle domain binds to FliM middle domain. It appears that the FliG C-terminal domain is responsible to pulling together two FliM monomers by interacting with the adjacent molecule.

CheY WT (inactive) and phosphono-CheY affect FliM-FliM oligomerization (Figure 3.8 and 3.11). When labeled FliMnm167C is in the absence of CheY and in the presence of WT FliGmc, two species are present in the population, one at short distance and one at long distance. The addition of WT CheY changes the distribution of these species. More short distance distribution is observed suggesting that FliM oligomer is formed while the long distance decreases suggesting a rearrangement of the FliM subunits. The occupation increase in the short distance distribution indicates that the two spin labels from two molecules are coming close together. Because FliMnm167 is located on α1', a close separation between two 167 sites suggests that a dimer very similar to the one in the crystal structure is being formed in the presence of phospho-CheY.

In the case of FliMnm121 (located at FliM α3) there are spin-spin separations only at long distance, where as for FliMnm60C

(located at α1) we observe well-separated distances at both short and long distance. In FliMnm121, oligomerization of FliM exists even in the absence of CheY, opposite to the case of FliMnm60, which shows very little oligomer in the absence of CheY. Since, FliMnm60 is located at the interface of the crystallographic dimer and the population at short distances increases with phosphono-CheY, we suggest that in the presence of phosphono-CheY (activated) the population of the crystallographic dimer increases. More details about FliM self-association will be discussed in the next chapter.

FliG c-terminal re-arrangement

During these experiments spin labeled FliGmc are used in the presence of unlabeled FliM. Both FliMmc spin label sites are located at the C-terminal domain. In both cases, FliG self-assembles independently of the presence of CheY and its activation state. In the case of FliG274, this spin label is located in the helix next to the helix in FliGc that has charged residues that interact with the stator (MotAB) and thus, are important for flagellar rotation. When activated CheY (i.e. phosphono-CheY) is added the population of species that give FliG-FliG distances from this position decreases. In contrast, when phosphono-CheY is added to FliG305 in the presence of WT FliM, the signal increases and more of these oligomer species are observed. These observations suggest that the FliG C-terminal domain undergoes subunit rearrangement. Interestingly, this data agrees with Blair's cross-linking experiments of the FliG C-terminal domain [21].

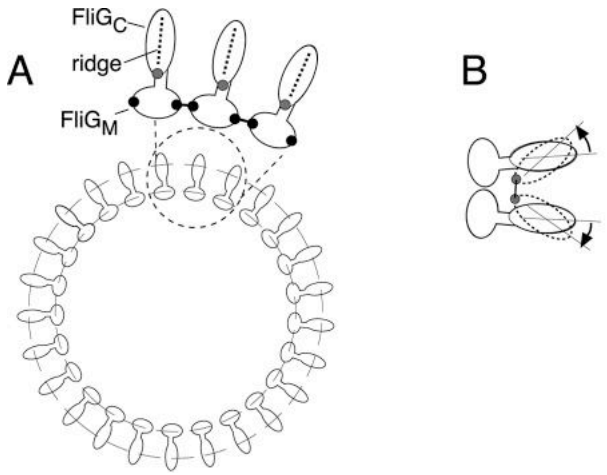

Figure 3.14 Blair's hypothesis based on small rotation of FliCc agrees with the ESR data. A) Overall arrangement of FliG subunits flagellum. B) Rotation of FliGc bringing together positions 297, 298, and 299, which are close to the residue spin-labeled 305. The location of residue 274 is close to the region of FliGc that moves farther apart (see arrows). Figure from [21].

They obtain the highest yield of cross-linking between residues that are close to position 305 on one end of the ridge. They explain the difference in cross-linking yield at the opposite ends of the ridge by suggesting that residues close to FliG305 comes together while simultaneously residues close to FliG274 are brought apart in a small rotation-like movement (Figure 3.14).

REFERENCES

1. Brown, P.N., C.P. Hill, and D.F. Blair, *Crystal structure of the middle and C-terminal domains of the flagellar rotor protein FliG.* EMBO J, 2002. **21**(13): p. 3225-34.
2. Minor, Z.O.a.W., *Processing of X-ray Diffraction Data Collected in Oscillation Mode*. Methods Enzymol, ed. J.R.M.S. C.W. Carter. Vol. 276. 1997, New York: Academic Press.
3. McCoy, A.J., et al., *Phaser crystallographic software.* J Appl Crystallogr, 2007. **40**(Pt 4): p. 658-674.
4. Brunger, A.T., et al., *Crystallography & NMR system: A new software suite for macromolecular structure determination.* Acta Crystallogr D Biol Crystallogr, 1998. **54**(Pt 5): p. 905-21.
5. Hubbell, W.L., et al., *Recent advances in site-directed spin labeling of proteins.* Curr Opin Struct Biol, 1998. **8**(5): p. 649-56.
6. Jeschke, G. and Y. Polyhach, *Distance measurements on spin-labelled biomacromolecules by pulsed electron paramagnetic resonance.* Phys Chem Chem Phys, 2007. **9**(16): p. 1895-910.
7. Borbat, P.P., R.H. Crepeau, and J.H. Freed, *Multifrequency two-dimensional Fourier transform ESR: an X/Ku-band spectrometer.* J Magn Reson, 1997. **127**(2): p. 155-67.
8. Borbat, P.P., H.S. McHaourab, and J.H. Freed, *Protein structure determination using long-distance constraints from double-quantum coherence ESR: study of T4 lysozyme.* J Am Chem Soc, 2002. **124**(19): p. 5304-14.

9. Park, S.Y., et al., *Reconstruction of the chemotaxis receptor-kinase assembly.* Nat Struct Mol Biol, 2006. **13**(5): p. 400-7.
10. Borbat, P.P. and J.H. Freed, *Measuring distances by pulsed dipolar ESR spectroscopy: spin-labeled histidine kinases.* Methods Enzymol, 2007. **423**: p. 52-116.
11. Park, S.Y., et al., *Structure of FliM provides insight into assembly of the switch complex in the bacterial flagella motor.* Proc Natl Acad Sci U S A, 2006. **103**(32): p. 11886-91.
12. Bhatnagar, J., J.H. Freed, and B.R. Crane, *Rigid body refinement of protein complexes with long-range distance restraints from pulsed dipolar ESR.* Methods Enzymol, 2007. **423**: p. 117-33.
13. Passmore, S.E., R. Meas, and D.L. Marykwas, *Analysis of the FliM/FliG motor protein interaction by two-hybrid mutation suppression analysis.* Microbiology, 2008. **154**(Pt 3): p. 714-24.
14. Brown, P.N., et al., *Mutational analysis of the flagellar protein FliG: sites of interaction with FliM and implications for organization of the switch complex.* J Bacteriol, 2007. **189**(2): p. 305-12.
15. Togashi, F., et al., *An extreme clockwise switch bias mutation in fliG of Salmonella typhimurium and its suppression by slow-motile mutations in motA and motB.* J Bacteriol, 1997. **179**(9): p. 2994-3003.
16. Irikura, V.M., et al., *Salmonella typhimurium fliG and fliN mutations causing defects in assembly, rotation, and switching of the flagellar motor.* J Bacteriol, 1993. **175**(3): p. 802-10.
17. Marykwas, D.L., S.A. Schmidt, and H.C. Berg, *Interacting components of the flagellar motor of Escherichia coli revealed by*

the two-hybrid system in yeast. J Mol Biol, 1996. **256**(3): p. 564-76.

18. Tang, H., T.F. Braun, and D.F. Blair, *Motility protein complexes in the bacterial flagellar motor.* J Mol Biol, 1996. **261**(2): p. 209-21.
19. Toker, A.S., M. Kihara, and R.M. Macnab, *Deletion analysis of the FliM flagellar switch protein of Salmonella typhimurium.* J Bacteriol, 1996. **178**(24): p. 7069-79.
20. Cornish, V.W., et al., *Site-specific incorporation of biophysical probes into proteins.* Proc Natl Acad Sci U S A, 1994. **91**(8): p. 2910-4.
21. Lowder, B.J., M.D. Duyvesteyn, and D.F. Blair, *FliG subunit arrangement in the flagellar rotor probed by targeted cross-linking.* J Bacteriol, 2005. **187**(16): p. 5640-7.

CHAPTER 4

MODELING THE FLAGELLAR MOTOR SWITCHING MECHANISM

4.1 FliM, FliN and FliG location

Three-dimensional (3D) maps of the flagellar rotor are available thanks to the collection of electron cryomicrographs images. Using these images and all the mutational, biochemical and x-ray crystallographic data available, we are able to suggest a model for the flagellar motor switching mechanism. It is not well understood yet where exactly in the motor all these components are located. A consensus mechanism cannot be proposed because too many variables need to be taken into consideration such as variations within bacterial species, whose flagellar architecture might change depending on location and number of flagella, which flagellar motor components are present in their genome and even the type of motility employed.

There is a very long observed and studied (even impressive) image of the flagellar motor that I have not shown until now (Figure 4.1a). This figure shows several main structures of the flagellar motor, including the C-ring where the switch complex is located. The C-ring looks like a drum-shape feature. The area that looks like a distorted Y-shape, is predicted to be the switch complex. Scientists suggest that the thinner region must me FliM, while the large blub or donut shape area must be FliN tetrater (oligomer seen in solution). The region on the top seems to have more than one domain and has been implicated to be FliG. At this location FliG can interact simultaneously with the MS (next structural feature seen above), with the FliM and the stator.

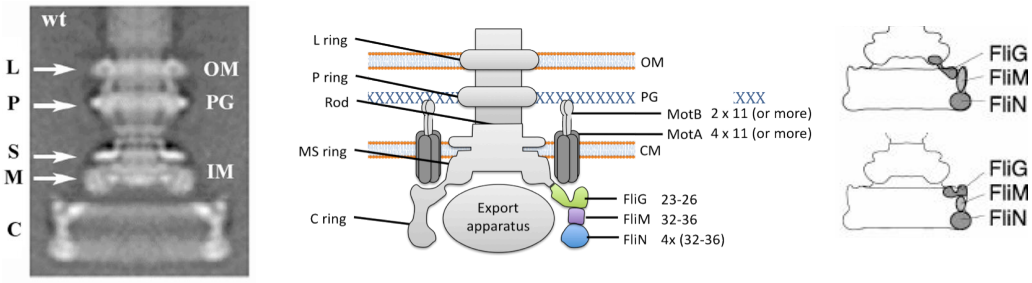

Figure 4.1 Ultrastructure of the flagellar basal body. A) EM average image of a single basal body of *Salmonella* showing the different structural features[1]. B) Schematic view of the flagellar basal body based on the EM image, roughly guessing where each of the flagellar switch complex components are located. C) Two hypothesis: #1(on top)- C terminal FliG makes up the inner lobe of the C-ring while the outer lobe would be a domain of FliM and #2 (lower one)- motor domain of FliG is in the outer lobe of the C-ring, where it can interact with both FliM and MotAB. [2-5]

In both hypothesis 1 and 2 (Figure 4.1c), they placed only FliGc interacting with FliMm while in hypothesis #2, FliGm is interacting with the MS ring. Based on our studies, we suggest that FliGm be located on top of FliM, while FliGn is interacting with the MS ring. FliGc is more difficult to locate in an EM average image, since we suspect that FliGc sometimes interacts with FliMm and sometimes directly with MotAB. Also, there may be molecules with one conformation (down interacting with FliM) while other molecules will have the more up-conformation interacting with MotAB.

People have been underestimating the size and occupancy of FliG N-terminal domain. These hypotheses are not taking in

consideration more than 100 residues that are not present in the FliGmc crystal structure. This domain might be the one responsible for most of the density in the EM images located close to the MS ring. A very recent EM study on *Borellia*, suggests for the first time the location of FliGn.

4.2 Molecular Mechanism of Flagellar Motor Switching

Chemotaxis is an amazing signaling transduction system that allows the bacterium to detect and respond to extremely small changes in stimulus over a wide range of background intensity with high sensitivity [6]. Biological sensing and regulatory systems are effective because of two properties, the ability to generate amplified responses to low levels of stimuli and the ability to adapt to changing levels of stimuli. During amplification, enhancement of the signal is involved. When the system is more sensitive to stimulus than the usual type of Michaelis-Menten binding (hyperbolic sensitivity) then it is called ultrasensitive [7]. Is very characteristic of ultrasensitivity to have a steep input-output relation [8]. A molecular mechanism for achieving ultrasensitivity is cooperativity. One possible source of cooperativity is at the level of the flagellar motors where CheY-P binding might be involved [9].

Cluzel *et al.* studied the bias of individual motors in single cells as a function of CheY-P concentration [8]. They found that when CW bias for individual cells was plotted versus the internal concentration of CheY-P it showed a sigmoid curve very distinctive of ultrasentivitity. Having ~34 FliM molecules in the switch, this can be visualize as

having ~34 binding sites for CheY. A cooperative binding process between CheY-P molecules and FliM could provide an explanation to the threshold effect, however Cluzel's experiments did not provide enough information to discern if the binding of CheY-P to the motor causes the amplification or if amplification happens within the switch itself. Research studies from the Eisenbach and Berg labs, found no cooperative binding of CheY-P to the switch suggesting that the chemotactic signal is indeed amplified within the switch [10, 11]. An allosteric transition between the rotational states of the switch is suggested. The uniformity of the motor characteristic suggests that some of the structural features of the motors may be rather tightly regulated. In this aspect an allosteric transition model, like the one suggested by the Berg lab, would make sense.

In this section, I will make the case that we are approaching understanding the structural elements within the flagellar switch complex that provide an explanation for how cooperativity maybe generated within the motor. Ultimately, the signal must travel trough the cytoplasm and reach the flagellar motor exactly at the switch complex in order to induce a change in the rotation of the flagella. This signal also has to be terminated in order to go back to pre-stimulus state and be able to sense the most minimum change in the environment. Other chemotaxis components are in charge of the termination of the signal and their involvement will not be discussed in this section. I will mostly focus on the signal-amplification-output based on the x-ray crystallography and ESR experiments reported in this dissertation and also the collection of data already published.

Amplification at the switch level: Implications of FliM self-association

As shown in Chapter 2, FliM self-associates both in-solution and in the crystal structure. The ESR data in this study provides evidence to suggest a symmetric dimer where each monomer is interacting through similar surfaces. This dimer could resemble the antiparallel dimer seen in our structure. This conclusion is based on the short distance distributions formed in the presence of CheY activated or inactive depending on the position of the label. It is still challenging to visualize how FliGm could be located at opposite sides, given the current understanding of the switch complex assembly state. It might suggest that only a few dimers are arranged antiparallel while the others are either parallel facing same faces or parallel facing the opposite face. The re-arrangement and disengagement of the FliM dimers could be a drastic large-scale re-orientation that could produce the change of direction of flagellar rotation or switching.

We have mutational and crosslinking data that suggests the FliM self-association interface is $\alpha 1$ in one monomer and $\alpha 2'$ in the other monomer (Figure 4.2) [12]. Efficient crosslinking of residues 57/185 and 64/185 Cys pairs, located in these two helices, indicates that adjacent FliM subunits in the C-ring are in close contact through these residues in an arrangement where they are parallel and facing opposite sides to form a chain of self-associated FliM monomers. It may be that both parallel and antiparallel dimers co-exist and correlate to CW or CCW states. In E.coli, for example, CheY-P has a preference to CW motors.

In a model of FliMm/FliGm195, where the FliM self-associates in the same way proposed by Park et al., the position of the FliGm195 agrees very well with the crosslinking experiments done by the Blair lab (Figure 4.2)[4]. Residues that show efficient crosslinking are located in helices A and E. The spacing between the FliGm195 subunits is within the typical separation between β-carbons of di-sulfide-bonded Cys residues.

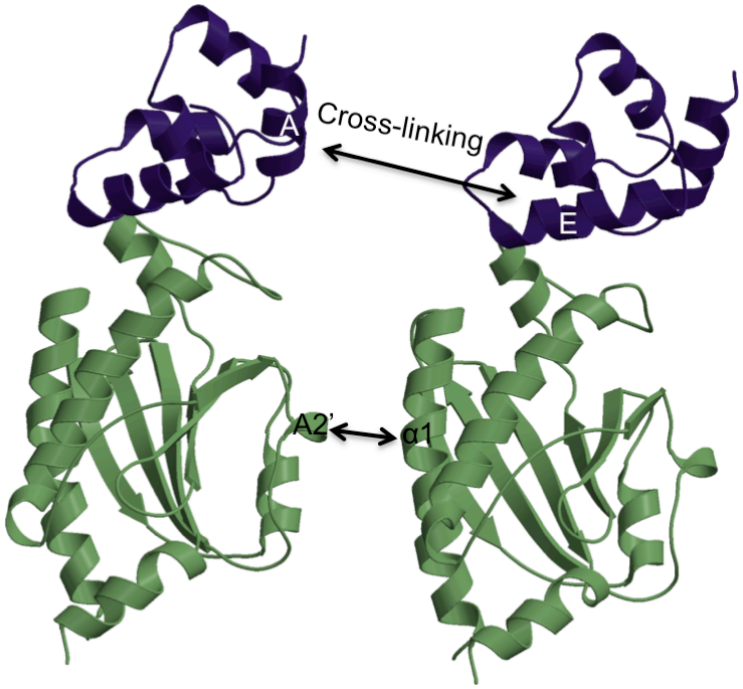

Figure 4.2 ModelI:Assembly of FliMm and FliGm195 based on Park et al. model for FliM assembly. Previous crosslinking experiments have suggested that FliM (blue) self-assembly interface includes specific residues on α2' and α1. If FliGm195 (pink) is added to the FliM-FliM model keeping the interactions at FliM loop α3-α1' (just like the structure) then FliGm195 proximity agrees with Blair's crosslinking interactions FliG. Crosslinking between the residues 117 and 120 on A and 166 and 170 on E are within the range for a disulfide bond, if FliG is fixed by the FliM interactions.

The binding of CheY-P might induce conformational changes in FliM. How can we couple the CheY-P binding event with signal propagation from FliM to FliG in order to trigger the switch between CW and CCW? And how is then this signal propagated from FliG to the stator MotAB in order to generate torque? The following new model addresses these issues.

Previous flagellar switch complex models

The flagellar switch complex is being extensively studied by several research groups, providing a large amount of data from crosslinking experiments, yeast hybrid assays, EM, x-ray crystallography, etc. Despite all this effort, the mechanism of how CheY-P switches the motor remains uncertain. It is substantial challenge to organize all this information in order to determine where each component of the switching located and how through direct or indirect interactions and how CheY-P affects these interactions.

It is known that CheY-P is the cytoplasmic component that contacts FliM in the switch complex. Many studies, including NMR and x-rays crystallographic studies, focus on the conserved FliM N-terminal domain peptide (first 16 residues) as a domain of interaction with CheY. Recent NMR studies, reported for the first time another site of interaction on FliM for CheY binding [13]. This data found that hydrophobic patch at the C-terminus of $\alpha 2$ helix on FliM serves as another site of interaction for CheY (Figure 4.3). As mentioned before, this $\alpha 2$ is involved in FliM-FliM interaction. There is a shared region on FliM that during the NMR studies is found to be perturbed by both

FliGc and activated CheY. Based on these observations they proposed a molecular mechanism of CheY-promoted switching where FliGc interacts with FliMm and then gets displaced after the interaction of CheY with the same region.

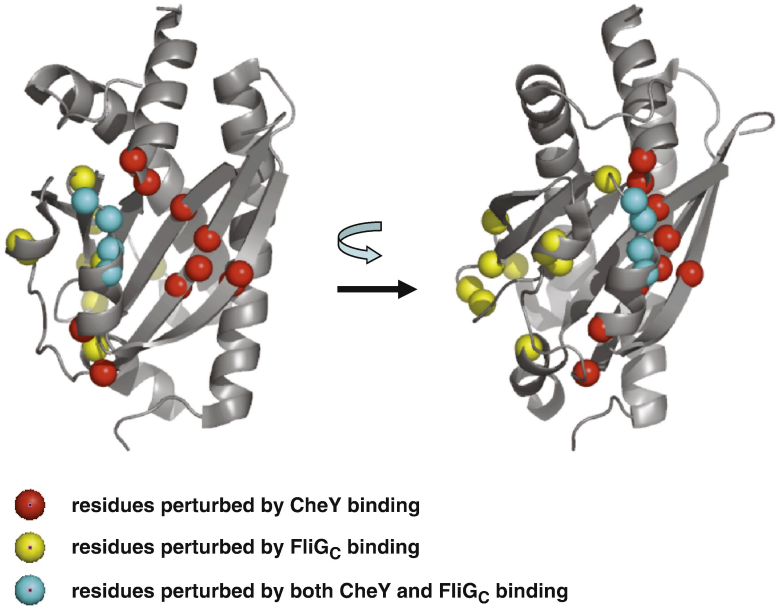

Figure 4.3 FliM regions of interaction. A shared surface of FliMm is affected when CheY and FliGc bind. Regions perturbed during NMR studies when activated CheY binds are shown as red spheres. The ones perturbed by FliGc are yellow spheres and the ones shares by both are cyan spheres. This figure was taken from [13].

New Flagellar switching model

Our crystal structure and biochemical studies provide new insights into a more complete model for the molecular mechanism of flagellar motor switching. First, the FliMm and FliGc195 molecules are arranged as described previously. For easier visualization, Figure 4.4, shows a chain of three FliMm molecules each in complex with

FliGm195. The FliG C-terminal domain (FliGc) is modeled into the crystal structure of FliMm/FliGm195. Two of the FliGc are modeled interacting with the adjacent FliMm. Based on FliM and FliG stoichiometry (26 FliG and 34 FliM) 1/3 of the FliG should interact with two FliM molecules. FliMm must be occupied first by FliGm since this domain contains the high affinity binding site and EHPQR binding motif. The interaction of the 1/3 FliG molecules with an adjacent FliM through the lower affinity binding site on FliGc may be involved in stabilization of the FliM-FliM oligomerization holding adjacent subunits together. This assumption might explain why during ESR experiments FliM oligomerization was observed in solution only when both the middle and C-terminal domains of FliG were present. I note that based on the stoichiometry and low/high affinity binding sites, most FliGc must be interacting by default the stator.

When activated CheY (CheY-P) binds to FliM N-terminal peptide (FliMn) it gets recruited towards the middle domain of FliM taking advantage of the flexible linker between FliMn and FliMm. The spatial orientation of this interaction is in the inner feature of the C-ring. When CheY binds to FliMm it induces a re-arrangement of FliGc. FliG C-terminal domain then interacts with the stator. In order to interact with MotAB, FliGc has to move from the inner section of the C-ring to the more outer surface of the C-ring. This model agrees that the surface of interaction of FliGc with FliM is oriented in opposite side to the conserved charge residues that interact with MotA.

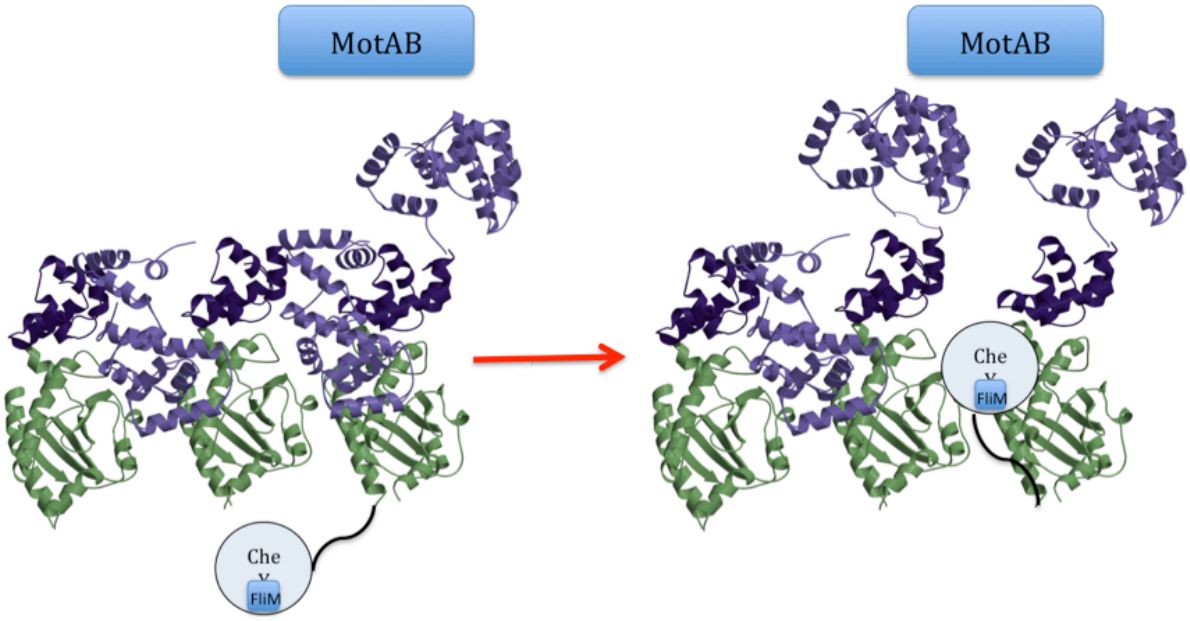

Figure 4.4 Proposed molecular mechanism of CheY-promoted flagellar motor switching The FliG C-terminal domain (FliGc) is modeled into the crystal structure of FliMm/FliGm195. Two of the FliGc are modeled interacting with the adjacent FliMm. As the concentration of CheY~P increase, CheY-P interacts with FliMn and then with FliMm. The interaction of CheY-P with $FliM_M$ displaces the FliGc domain from its binding site on $FliM_M$. This requires a large-scale reorientation of the FliGc domain, modifying the proximal surface of FliGc relative to the stator components that generate torque and are anchored to the membrane and peptidoglycan. This event might reverse the rotational sense of the motor.

If the re-arrangement is more like a flip motion, the right surface of interaction will be accessible for the stator. This movement of FliGc might be possible thanks to the flexible linker that connects this domain to FliGm. This flexibility is unique feature due to the existence of two highly conserved Gly residues between the linker and FliGc. It is still debatable if FliGc domain movement is a complete displacement as Dyer et al. suggests, or if it is more likely to be a subtle

displacement as the ESR and crosslinking experiments suggest. Either way movement of this domain could be responsible for the switching mechanism.

We suggest that the binding of CheY-P at FliM interface can be expected to affect motor bias, probably affecting the arrangement of the FliM oligomer state and position of the FliGc binding domain. ESR experiments suggest that CheY and CheY-P produce a re-arrangement of FliM molecules sometimes increasing the population of FliM-FliM oligomers.

4.3 Conclusion

One thing to note is that these models are derived from speculations based on the crystal structures of fragments of the switch complex components. Not only they are not full-length structures but also they are from *Thermotoga maritima*, while most of the EM images are from other organisms. Moreover, the oligomeric states found in the crystal structure often assumed to be relevant to the intact motor, and this is debatable. We are still in the need of more full-length crystal structures of the components and also crystal structures of more complexes. More crystal structures in combination with well developed and advanced imaging techniques such as electron cryomicrography will be crucial in order to understand where these components are located. Also it is about time to look more closely at other bacterial species.

REFERENCES

1. Thomas, D., D.G. Morgan, and D.J. DeRosier, *Structures of bacterial flagellar motors from two FliF-FliG gene fusion mutants.* J Bacteriol, 2001. **183**(21): p. 6404-12.
2. Blair, D.F., *Fine structure of a fine machine.* J Bacteriol, 2006. **188**(20): p. 7033-5.
3. Thomas, D.R., et al., *The three-dimensional structure of the flagellar rotor from a clockwise-locked mutant of Salmonella enterica serovar Typhimurium.* J Bacteriol, 2006. **188**(20): p. 7039-48.
4. Lowder, B.J., M.D. Duyvesteyn, and D.F. Blair, *FliG subunit arrangement in the flagellar rotor probed by targeted cross-linking.* J Bacteriol, 2005. **187**(16): p. 5640-7.
5. Brown, P.N., C.P. Hill, and D.F. Blair, *Crystal structure of the middle and C-terminal domains of the flagellar rotor protein FliG.* EMBO J, 2002. **21**(13): p. 3225-34.
6. Spiro, P.A., J.S. Parkinson, and H.G. Othmer, *A model of excitation and adaptation in bacterial chemotaxis.* Proc Natl Acad Sci U S A, 1997. **94**(14): p. 7263-8.
7. Koshland, D.E., Jr., A. Goldbeter, and J.B. Stock, *Amplification and adaptation in regulatory and sensory systems.* Science, 1982. **217**(4556): p. 220-5.
8. Cluzel, P., M. Surette, and S. Leibler, *An ultrasensitive bacterial motor revealed by monitoring signaling proteins in single cells.* Science, 2000. **287**(5458): p. 1652-5.

9. Kuo, S.C. and D.E. Koshland, Jr., *Multiple kinetic states for the flagellar motor switch.* J Bacteriol, 1989. **171**(11): p. 6279-87.
10. Sagi, Y., S. Khan, and M. Eisenbach, *Binding of the chemotaxis response regulator CheY to the isolated, intact switch complex of the bacterial flagellar motor: lack of cooperativity.* J Biol Chem, 2003. **278**(28): p. 25867-71.
11. Sourjik, V. and H.C. Berg, *Binding of the Escherichia coli response regulator CheY to its target measured in vivo by fluorescence resonance energy transfer.* Proc Natl Acad Sci U S A, 2002. **99**(20): p. 12669-74.
12. Park, S.Y., et al., *Structure of FliM provides insight into assembly of the switch complex in the bacterial flagella motor.* Proc Natl Acad Sci U S A, 2006. **103**(32): p. 11886-91.
13. Dyer, C.M., et al., *A molecular mechanism of bacterial flagellar motor switching.* J Mol Biol, 2009. **388**(1): p. 71-84.

APPENDIX A

BACTERIAL CHEMOTAXIS STUDIES IN DIFFERENT BACTERIAL MODELS

Flagellar homologues

A good strategy to study and reconstitute the switch complex is to use proteins from different organisms and also clone fragments of different lengths. This strategy can increase the chances of successful crystallization. I have cloned, expressed and purified several frangments and full length constructs of FliM, FliN, FliG and FliY (FliY/N) from *Thermotoga maritima* (TM), *Bacillus subtilis* (BS) and *Geobacillus stearothermophilus* (GS). Stable complexes of FliM/FliN, FliM/FliN/FliY and FliM/FliN/FliG have been produced and characterized (Figure A1a). Tables A1 and A2 show a summary of the fragments successfully cloned, expressed and/or purified. Figure A1a shows different complexes and how well they behave in solution. Figure A1b, shows a size exclusion chromatography profile characterizing different full length constructs from BA and GS.

In addition to the flagellar switch complex components, I also cloned, expressed and purified the response regulator CheY from TM and BS. The full length FliY from *Bacillus anthracis* was provided by our collaborators in the Ordal lab in University of Illinois at Urbana Champaign (see Appendix B for more information).

Table A1 Flagellar Switch Complex full length and fragment components cloned from *Thermotoga maritima* using different expression vectors

Construct	Residues	MW (kDa)	Vector
$TMFliM_{FL}$	1-328	37.9	pET28
$TMFliM_{FL}$	1-328	37.9	pAED4
$TMFliM_{242}$	1-242	16.6	pET28
$TMFliM_{249}$	1-249	17.3	pET28
$TMFliM_{-45}$	46-242	22.8	pET28
$TMFliM_{C}$	44-226	21.0	pET28
$TMFliM_{N}$	252-328	8.6	pET28
TMFliN	1-154	17.6	pET28
TMFliN	1-154	17.6	pSBETa
TMFliN	1-154	17.6	pAED4
TMFliN	23-154	15.1	pET28
TMFliN	23-154	15.1	pSBETa
TMFliG	1-184	20.6	pJY5
TMFliG	1-170	18.9	pJY5
TMFliG	1-195	21.9	pSK8
TMFliG	1-195	21.9	pAED4
TMFliG	104-334	26.2	pSK8
TMFliG	104-334	26.2	pET16.b
TMFliGm	117-169	5.9	pET28
TMFliGm	117-195	8.9	pET28
TMFliGc	180-335	17.8	pET28
TMFliGc	195-335	16.1	pET28
TMFliGc	209-335	14.7	pET28
$TMFliG_{MC}$	115-327	24.2	pET28
$TMFliG_{MC}$	115-327	24.2	pACYCDuet-1
$TMFliG_{MC}$	115-327	24.2	pSBETa
TMFliY	1-162	17.4	pET28
TMFliY	1-162	17.4	pACYCDuet-1
$TMFliY_{FL}$	1-343	38.0	pET28

A

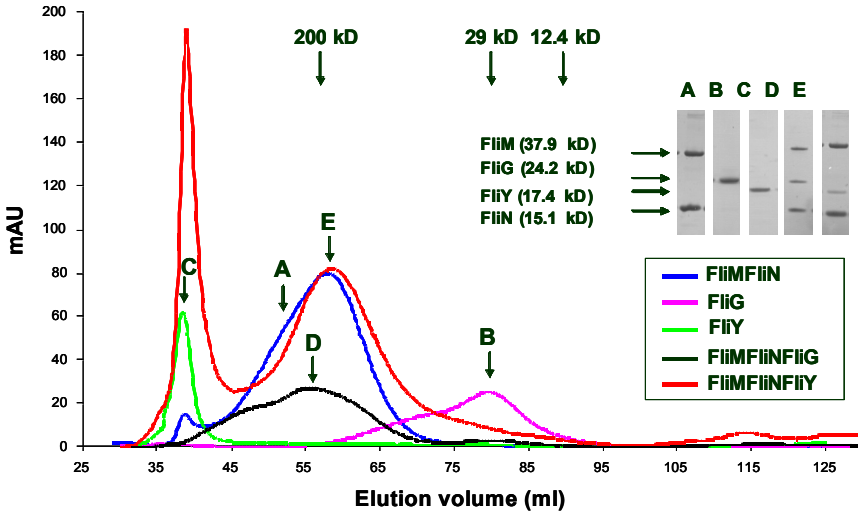

B

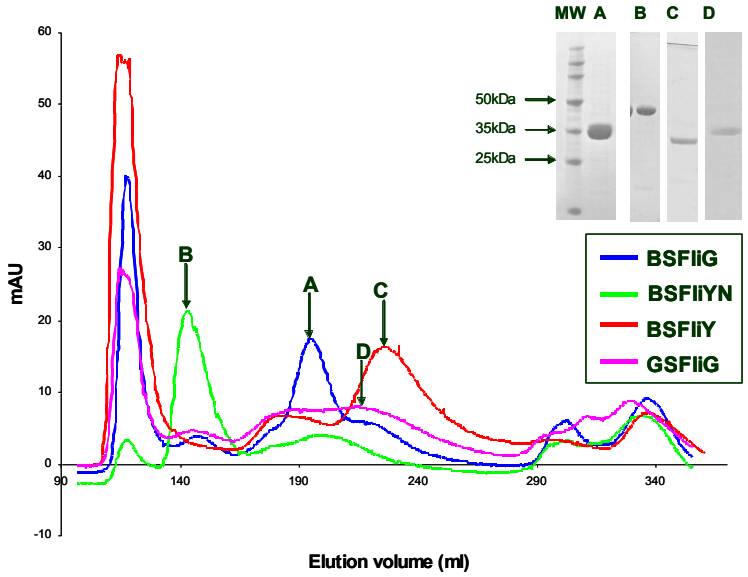

Figure A1 a) FliM/FliN, FliM/FliN/FliY and FliM/FliN/FliG complexes were reconstituted using size exclusion chromatography. b) Full length proteins in *Bacillus subtilis and g. stearothermophilus* behave express well even when some form aggregates (large void peak).

Table A2 Flagellar Switch Complex full length and fragment components and non-flagellar homologs cloned from *Bacillus subtilis, Geobacillus stearothermophilus, Bacillus anthracis* and *Myxococcus xanthus* using different expression vectors

Construct	Residues	MW (kDa)	Vector
BSFliM	1-332	37.5	pET28
BSFliG	1-338	38.2	pET28
BSFliY	1-378	41.1	pET28
BSFliY	1-186	19.8	pET28
BSFliN	187-378	21.2	pET28
BSFliN	237-378	15.7	pET28
GSFliM	1-334	37.8	pET28
GSFliG	1-339	38.2	pET28
GSFliY	1-393	42.0	pET28
BaFliY	1-546	61.0	pBluescriptSK
BaFliY	1-546	61.0	pET28
DifD	1-122	13.1	pQE-32
DifD	1-122	13.1	pET28
DifG	1-200	20.6	pQE32
DifG	1-200	20.6	pET28

Non-flagellar homologues

DifG is FliY/CheC/CheX homolog in *Myxococcus xanthus* while DifD has homology with CheY [1-3]. These genes are essential for gliding motility. There is evidence that suggests that DifD interacts with the CheA homolog DifE. It is unknown how DifD interacts with the gliding motors. Having a structure of DifG/DifD complex will be a major step forward in elucidating the phosphatase mechanism of

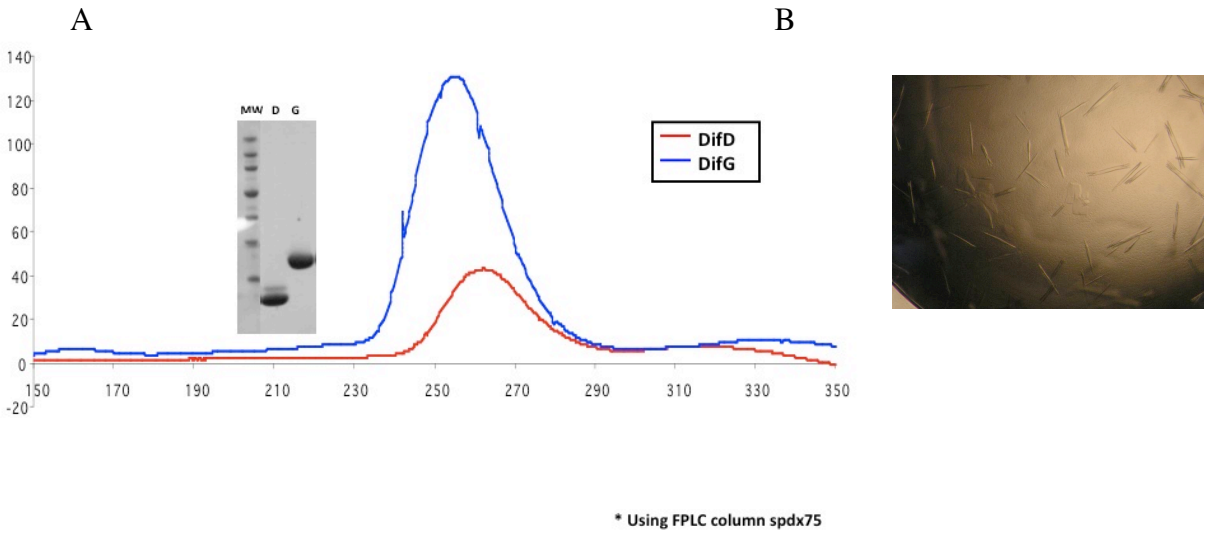

Figure A3 DifD and DifG protein purification and crystallization. a) Size exclusion chromatography profile and SDS gel of the profile peaks. b) Crystal needles of DifD and DifG in the presence of BeF^{3-}, 0.2 Ammonium sulfate and15% PEG4K.

CheC/CheX/FliY family. Our collaborators from Yang Lab at Virginia Polytechnical Institute provided these constructs. These proteins were expressed and purified (Figure A3a). Crystal needles were obtain from the a mix 1:1 of DifD and DifG in the presence of BeF^{3-} (Figure A3b) .

REFERENCES

1. Bonner, P.J., et al., *The Dif chemosensory pathway is directly involved in phosphatidylethanolamine sensory transduction in Myxococcus xanthus.* Mol Microbiol, 2005. **57**(5): p. 1499-508.
2. Yang, Z. and Z. Li, *Demonstration of interactions among Myxococcus xanthus Dif chemotaxis-like proteins by the yeast two-hybrid system.* Arch Microbiol, 2005. **183**(4): p. 243-52.
3. Black, W.P. and Z. Yang, *Myxococcus xanthus chemotaxis homologs DifD and DifG negatively regulate fibril polysaccharide production.* J Bacteriol, 2004. **186**(4): p. 1001-8.

APPENDIX B

THE FLIN/FLIY DILEMMA

The main goal of my research has being to reconstitute the flagellar switch complex. As mentioned previously, I have been able to reconstitute a stable complex composed of FliM, FliN and FliG from *Thermotoga maritima.* In this process, I discovered an overlooked feature of FliN protein.

The two flagellar switch proteins FliM and FliN have sequence homology with FliY, which is assumed to be localize at the flagellar basal body[1]. FliY gene was first isolated from *B. subtilis*, whose product shows similarities to both FliN anf FliM [2]. In this organism, FliN has being replaced by FliY, which is twice as longer and sometimes refered as to FliY/N. The last 100 residues at the C-terminus have sequence homology with *E.coli* FliN. A plasmid-borne fliY gene can restore motility to Salmonella fliN mutant, suggesting that FliY can function in the role of FliN [2]. The N-terminus domain is quite similar to the N-terminus domain of FliM, more specifically the residues 6-15. This region has being identified in FliM as CheY binding domain.

FliY and FliM also share structural homology with the CheY-P phosphatases, CheX and CheC. Phylogenic studies by Kirby *et.al.*, indicated a common ancestry for CheC/CheX proteins and flagellar switch protein FliM and FliY [3]. In *B. subtilis,* FliY/N functions as CheY-P phosphatase [4, 5]. As shown in Figure B2, FliM has a central domain homologous to CheC and a C-terminal domain homologous to

FliN. FliM lacks the EIGN dephosphorylation motif present in the CheC phosphatase family. FliM and FliY/FliN have a CheY-P binding domain that CheX and CheC lack. The structure of FliM central domain shares the same topology as the CheC phosphatase family (Figures B1 and B2) with a main difference in the α2 helix [6]. FliY is the only component of the flagellar switch complex whose crystal structure has yet to be determined. The exact location of FliY in the switch complex is unknown. Why there is phosphate located in the flagellar motor is also unknown. It has been hypothesize that FliY constitutively remove CheY-P around the flagellar switch to maintain CheY-P concentration at the optimum level [4].

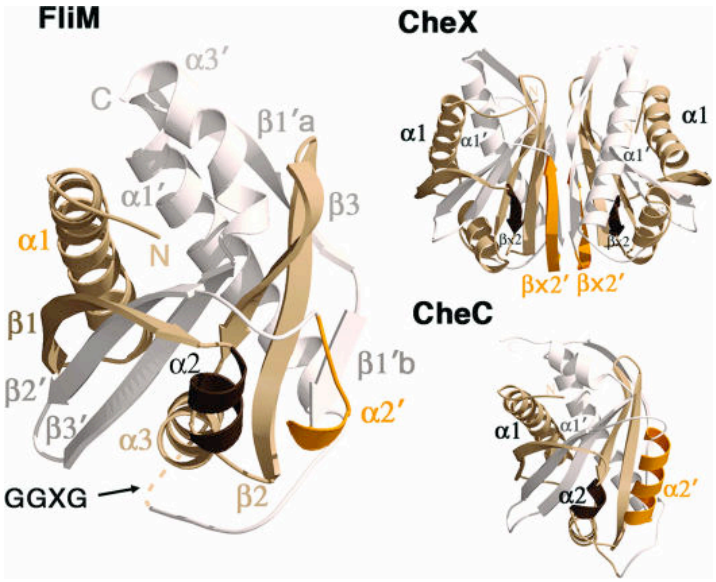

Figure B1 Structure of FliM reveals homology to the CheC/CheX phosphatase family. Pseudo-2-fold axes relate one-half of the monomer units (white) to the other (tan). The α2′/β_x′ regions (orange), which differ in structure among the three proteins, dimerize CheX, associate CheC with CheD, and mediate FliM self-interactions. The conserved, but disordered, GGXG motif links the two halves of FliM. Figure from [6].

Confusion can occur because genes for FliY/N fusion proteins can be annotated as either FliY, FliN, or FliY/N. We can find organisms with only FliN, only FliY/N and some even contain both FliN and FliY (Table 2B). In the case of *T.maritima,* the Blair lab cloned the FliN gene from FliY2 (one of two genes annotated as FliY).

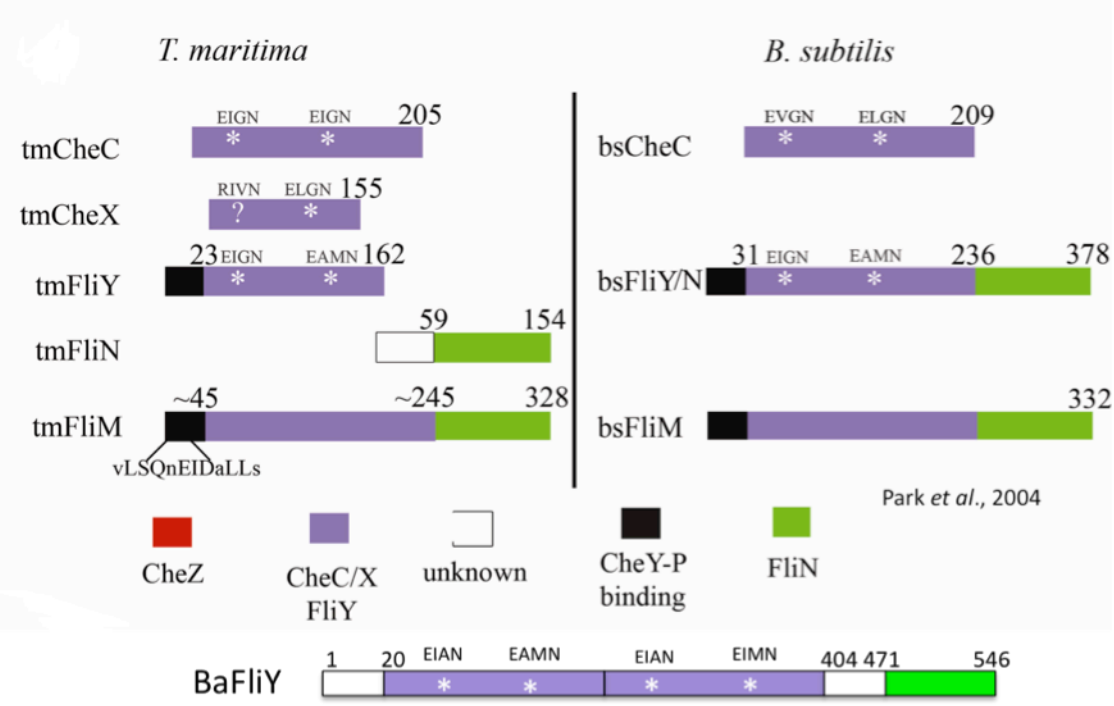

Figure B2 Domain organization for the CheC/CheX/FliY phosphatase family in *T.maritima, B.subtilis* and *B.anthracis.* Purple segments represent the CheC homology region; green segments represent the FliN homology region. FliY/N and FliM contain an N-terminal peptide that binds CheY-P (black). CheC, CheX, and FliY/N contain dephosphorylation centers (white stars with conserved residues above), but FliM does not. Most FliY/N proteins follow the domain architecture of bsFliY/N. TmFliY is being studied as a truncated protein

My recent cloning of full length FliY from *Thermotoga maritima* proved that there is a mistake in the annotation of the genome (Figure B3). The fliY gene is labeled as one with an authentic frameshift mutation, where one nucleotide is missing. Taking a closer look at the sequence as it is annotated, all reading frames result in stop signals impeding the expression of a full length protein. If a guanine nucletide is added as shown in Figure B4, then the sequence reads as complete transcribable gene. Primers were designed in order to add this nucleotide by PCR Quickchange mutation reaction using *T. maritima* genome DNA was performed. Interestingly, the clone which Quickchange mutation was not performed (no addition of nucleotide) also resulted in a full length FliY gene as well, indicating that the guanine was always present and the annotation was incorrect.

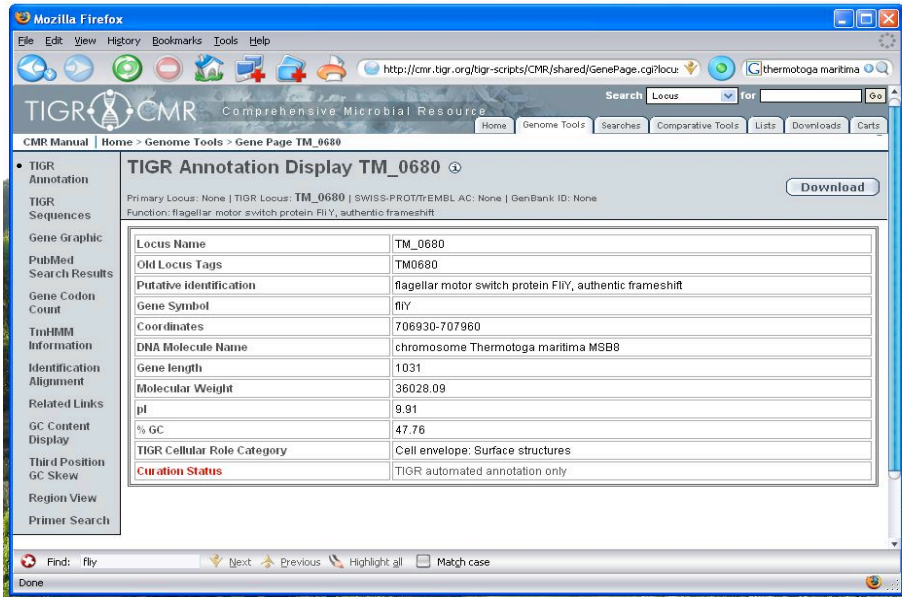

Figure B3 FliY is annotated as an authentic frameshif mutant. Print-screen of *Thermotoga maritima* MSB8 Genome webpage showing the still mistakenly annotated FliY.

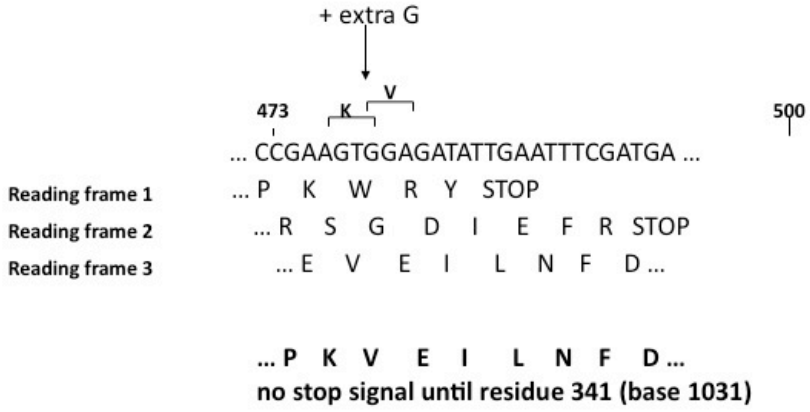

Figure B4 $FliY_{FL}$ cloning and mutation.

After cloning, expressing and purifing the full length FliY from *Thermotoga maritima*, stable complexes of FliM/$FliY_{FL}$ FliM/FliG/$FliY_{FL}$ were produced and characterized using size exclusion chromatography (Figure B5). All previous research on FliY is based on the short and mistakenly cloned gene. The new full length FliY resemble the fusion of the short FliY fragment and FliN. This finding revealed that FliN is actually the C-terminus of the full length FliY in *T.maritima* and not a individually expressed protein. Studying this full length FliY will provide better understanding of how CheY-P interacts with its phosphatases and also how CheY interacts with FliM to induce switching.

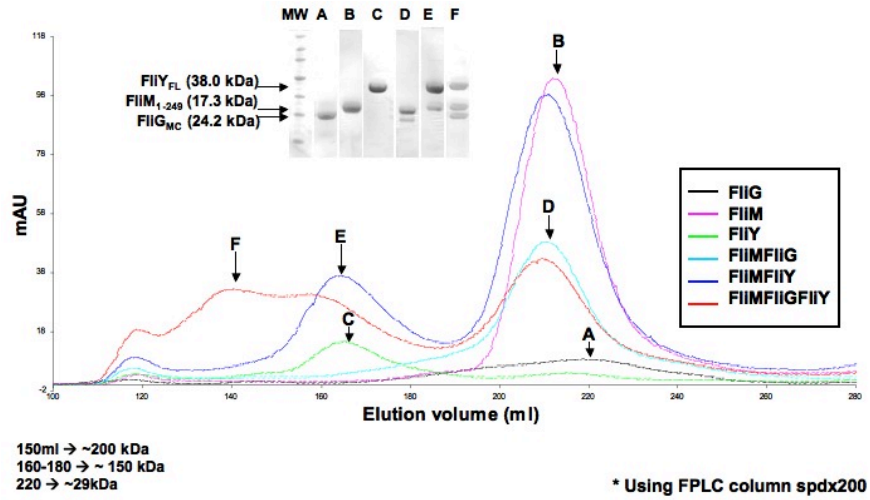

Figure B5 Size exclusion chromatography profiles of FliY full length and other flagellar switch complex components. These experiments provide evidence of interaction between the flagellar switch complex components using the new full length FliY.

Another FliY full-length fragment that I have studyed is from *Bacillus anthracis* , the expression plasmid for which was kindly provided by our collaborators in the Ordal lab in University of Illinois at Urbana Champaign. The gene of this particular FliY has two copies of the CheC-like domain (Figure B6). Small needle-like crystals were obtained for this construct (Figure B7). Several attempts were performed in order to increase the size and quality of these crystals. These attempts include use of different salts, buffers, pH, protein and precipitant concentration and use of macroseeding and additive screen In order to continue optimizing the BaFliY crystals, several fragments have been cloned (Table B1).

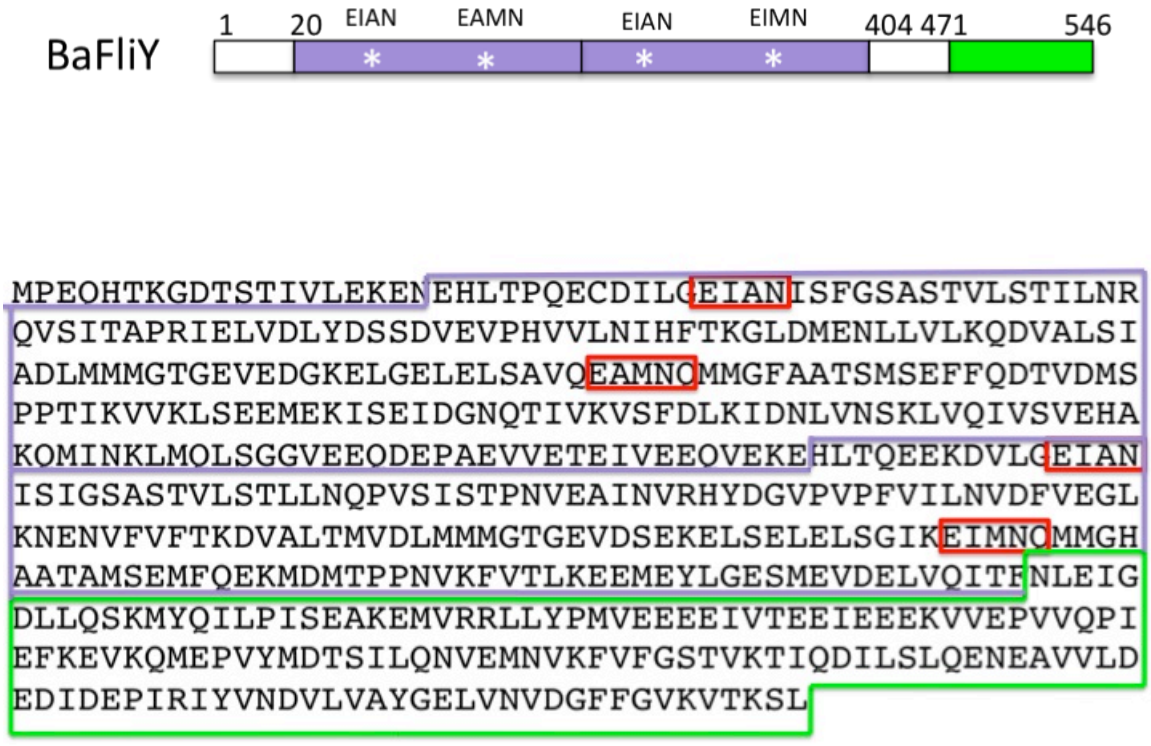

Figure B6 Bacillus anthracis has two CheC domains and one FliN domain. Two separate CheC domains (purple) and one FliN (green) can be identified after sequence analysis. This FliY then contains four separate phosphatase active sites (red).

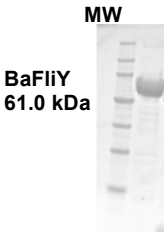

Figure B7 BaFliY crystal needles and SDS-PAGE gel showing highly pure and well express protein. Needles grew from 0.1 M K_2SO_4, 0.1M Tris pH 8 and 18 % PEG.

Table B1 Summary of re-cloning strategy of BaFliY. See Figure B6 for easier visualization

BaFliY clone	Residues	Strategy
BaFliY1	20-546	Starting where TMCheC homologous region until the end of sequence, eliminating the N-term which has no homology to TMFliM or TMFliY (no N-term CheY binding peptide).
BaFliY2	20-404	Starting at same position as BaFliY1 and ending right before the homology region with FliN starts.
BaFliY3	20-471	Starting at same position as BaFliY1 and 2 and ending right after the region (if aligned with FliN) that we don't have structural information for FliN
BaFliY4	1-404	Starting at residue #1 of the FL and ending right before homology region of FliN starts
BaFliY5	1-471	Also starting at residue #1 of the FL and ending right after the region of FliN that we don't have structural information

Table B2 Bacterial species predicted to contain both FliY and FliN [7]

Strain[a]	Accession no.[b]	
	FliY	FliN
Firmicutes		
Bacillus anthracis strain Ames	NP_844108.1	NP_844145.1
Bacillus cereus ATCC 10987	NP_978070.1	NP_978104.1
Bacillus thuringiensis serovar *israelensis* ATCC 35646	ZP_00740677.1	ZP_00743099.1
Bacillus thuringiensis serovar kondukian strain 97-27	YP_035851.1	YP_035883.1
Bacillus thuringiensis strain Al Hakam	YP_894318.1	YP_894349.1
Bacillus weihenstephanensis KBAB4	ZP_01183416.1	HP_01186704.1
Listeria innocua Clip11262	NP_470051.1	NP_470049.1
Listeria monocytogenes EGD-e	NP_464227.1	ZP_00232875.1
Listeria welshimeri serovar 6b strain SLCC5334	YP_848870.1	YP_848868.1
Carboxydothermus hydrogenoformans Z-2901	YP_359867.1	YP_359850.1
Moorella thermoacetica ATCC 39073	YP_429666.1	YP_429645.1
Epsilonproteobacteria		
Campylobacter coli RM2228	ZP_00367872.1	ZP_00367623.1
Campylobacter concisus 13826	ZP_013733.76	ZP_01374235.1
Campylobacter curvus 525.92	ZP_01806896.1	ZP_01806986.1
Campylobacter fetus subsp. Fetus 82-40	YP_892647.1	YP_891558.1
Campylobacter jejuni RM1221	YP_178081.1	YP_178419.1
Campylobacter lari RM2100	ZP_00368719.1	ZP_00368652.1
Campylobacter upsaliensis RM3195	ZP_00369881.1	ZP_00370648.1
Helicobacter acinonychis strain Sheeba	YP_664894.1	YP_665155.1
Helicobacter hepaticus ATCC 51449	NP_860679.1	NP_861108.1
Helicobacter pylori 26695	NP_207820.1	NP_207379.1
Helicobacter pylori HPAG1	YP_627158.1	HP_627304.1
Helicobacter pylori J99	NP_223113.1	NP_223249.1
Helicobacter pylori G27	YP_002266029.1	YP_002266028.1
Thiomicrospira denitrificans ATCC 33889	YP_393222.1	YP_393679.1
Wolinella succinogenes DSM 1740	NP_907768.1	NP_907256.1
Spirochaetales		
Leptospira borgpetersenii serovar Hardjo-bovis JB197	YP_800948.1	YP_797771.1
Leptospira interrogans serovar Lai strain 56601	NP_712794.1	NP_712250.1

[a] Bacteria that contain both FliY and FliN. Only one strain is listed if multiple strains of the same species all had similar FliY/FliN distributions, except in the case of the epsilonproteobacteria.

[b] NCBI reference sequence numbers (http://www.ncbi.nlm.nih.gov/protein/).

Recent studies in Helicobacter pylori, showed that both fliN and fliY are needed for wild-type levels of flagellation even when they are partially redundant [7]. The same group performed a protein sequence analysis to identify all microbial species carrying FliY proteins and which ones also contained FliN (Table B2). It will be interesting to characterize putative switch genes outside of the model organisms *E.coli, Salmonella* species and *B.subtilis*.

REFERENCES

1. Szurmant, H., et al., *Bacillus subtilis hydrolyzes CheY-P at the location of its action, the flagellar switch.* J Biol Chem, 2003. **278**(49): p. 48611-6.
2. Bischoff, D.S. and G.W. Ordal, *Identification and characterization of FliY, a novel component of the Bacillus subtilis flagellar switch complex.* Mol Microbiol, 1992. **6**(18): p. 2715-23.
3. Kirby, J.R., et al., *CheC is related to the family of flagellar switch proteins and acts independently from CheD to control chemotaxis in Bacillus subtilis.* Mol Microbiol, 2001. **42**(3): p. 573-85.
4. Szurmant, H., T.J. Muff, and G.W. Ordal, *Bacillus subtilis CheC and FliY are members of a novel class of CheY-P-hydrolyzing proteins in the chemotactic signal transduction cascade.* J Biol Chem, 2004. **279**(21): p. 21787-92.
5. Szurmant, H. and G.W. Ordal, *Diversity in chemotaxis mechanisms among the bacteria and archaea.* Microbiol Mol Biol Rev, 2004. **68**(2): p. 301-19.
6. Park, S.Y., et al., *Structure of FliM provides insight into assembly of the switch complex in the bacterial flagella motor.* Proc Natl Acad Sci U S A, 2006. **103**(32): p. 11886-91.
7. Lowenthal, A.C., et al., *Functional analysis of the Helicobacter pylori flagellar switch proteins.* J Bacteriol, 2009. **191**(23): p. 7147-56.

APPENDIX C

THERMOTOGA MARITIMA CHEY DEACTIVATION *

Introduction

CheY is the response regulator of the chemotaxis system. After phosphorylation by CheA, it travels through the cytoplasm until interacting with the switch complex of the flagellar motor to induce a change in the flagellar rotation. In order to return to the pre-stimulus state, CheY must loose the phosphate group. The CheY-phosphate is not stable. Even when it hydrolyzes in a short period of time (~20 seconds)[1], other proteins called phophatases are needed for a rapid termination of the signal. Whereas as E. coli contain a CheY phosphatase, CheZ, most other bacteria do not. Instead many bacteria contain CheC, CheX and CheD.

We have used phosphorylation assays and x-ray crystallography to determine that CheC and CheX are the phosphatases in *Thermatoga maritima*. CheC and CheX have a unique fold and active center compared to the other known phosphatase families (Figure C1). I showed using radioactive assays that CheC phosphatase activity is enhanced by CheD, which was known previously to deaminate glutamines in the receptor. Interestingly, CheX activity is stronger than CheC. My mutagenesis studies of CheC and CheX have implicated an essential Asn residue that has to be involved in CheY-P

* This data was published in part in [2]

dephosphorylation. CheC, CheX and CheD are found in a number of human pathogens that require chemotaxis to be infectious. Thus, these proteins signaling systems that mediate chemotaxis are potential targets for antimicrobial drug development against diseases such as Lyme disease.

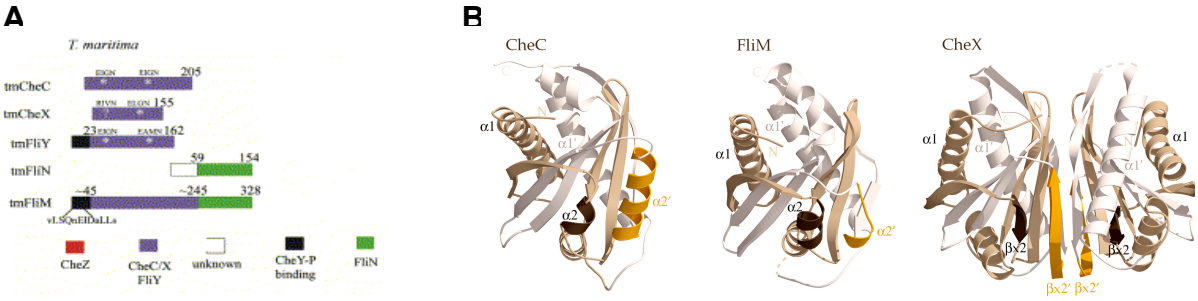

Figure C1 A) Domain organization for the CheC/CheX/FliY phosphatase family and FliM flagellar motor component, B) Crystal structures of FliM and the phosphatases CheC and CheX.

Methods and materials

Radioactive Dephosphorylation assays

CheA (18 μM) was autophosphorylated by incubation with 0.05 μM [γ-^{32}P] ATP (1.5 μl of 3000 Ci/mmol, 10 μCi/μl, Perkin-Elmer) and 20 μM cold ATP for 15 min in a total volume of 100 μl TKM buffer (50 mM Tris [pH 8.5], 50 mM KCl, 5 mM $MgCl_2$). The autophosphorylated CheA (CheA-^{32}P) was then added to premixed protein solutions, resulting in final concentration of 11.8 μM CheA-^{32}P, 32.9 μM CheY, 4.24 μM CheC (native or mutants), 6.1 μM CheD, or 2.8–5.6 μM CheX. After 3 min of incubation, 10 μl of 2× SDS buffer containing 50 mM EDTA was added

to quench each reaction. The proteins were separated on a 4%–20% Tris-glycine SDS-PAGE, and then transferred to an Immuno-Blot PVDF membrane (blotted for 30 min at 100 V using transfer buffer [25 mM Tris, 192 mM glycine]). The PVDF membrane was exposed to film and the film was later developed. Protein concentrations were taken from the calculated extinction coefficients at 280 nm based on aromatic amino acid content and verified by the RC/DC assay (BioRad). Equal concentrations of CheC mutants were assured by SDS-PAGE and the RC/DC assay.

Results and Discussion

Deactivation: Activities of CheC and CheX toward CheY-P

We tested the effects of T. maritima CheC, CheX, and CheD on *T. maritima* CheA-P and CheY-P. As typical of CheA proteins at 25°C, T. maritima CheA autophosphorylates itself prior to transferring phosphate to CheY (Figure C2A and C2B) Despite reports that B. subtilis CheC and CheA interact in a yeast two-hybrid assay, T. maritima CheC, CheX, and CheD had no effect on CheA autophosphorylation or dephophosphorylation. We also saw no evidence for CheC, CheD, or CheX phosphorylation by CheA or CheY. However, CheX and CheC (but not CheD) dephosphorylated CheY, with CheX having greater activity than CheC (Figure C2B). On addition of CheD, CheC activity increased substantially and dephosphorylated all of the CheY-P present in our assay. At the shortest time measured, both CheX and CheC/CheD depleted not only all of the CheY-P but also all of the CheA-P, which likely results from a large increase in the

steady-state concentration of unphosphorylated CheY (FigureC2B). We were unable to detect an effect of CheC or CheX on the T. maritima CheB methylesterase (which contains a CheY-like domain), due to the short lifetime of CheB-aspartyl-phosphate (data not shown).

CheC single-point mutants of Glu13, Asn16, Glu112, or Asn115 (all to Ser) and the double mutants, Glu13Ser/Glu112Ser and Asn16Ser/Asn115, all reduced CheY phosphatase activity to a nearly undetectable amount (i.e., increased CheY-P in the assay to a level similar to that seen with no CheC present) (Figure C2). Thus, because of low CheC activity in the absence of CheD, it is difficult to distinguish the effects of the single mutants from those of the double mutants (data not shown). However, on the addition of CheD, activities of all single mutants increase to levels greater than that of wild-type CheC alone, and differential effects of the double mutants become apparent (Figure C2B and C2C). In the presence of CheD, the Asn115Ser mutant displays less activity than wild-type or the Asn16Ser mutant, but more activity than the Asn16Ser/Asn115Ser double mutant, which shows little or no activity (Figure C2B and C2C). The Glu13/Glu112 double mutant also has reduced activity in the presence of CheD, but exceeds the activity of CheC alone (Figure C2B and C2C). Both CheC double mutants, Glu13/Glu112 and Asn16/Asn115, have the same affinity for CheD as wild-type (dissociation constant K_D = 0.9–1.4 μM, and stoichiometry n = 0.85–1.1 CheC/CheD by isothermal titration calorimetry); thus, these conserved residues do not solely mediate activation by binding CheD.

Figure C2 Activities of *T. maritima* CheC, CheX, and CheD*
(A) Flow of phosphate followed in the experiments shown in (B)–(C).
(B) Autophosphorylated CheA (CheA-^{32}P) in the absence or presence of CheY, CheC, CheD, CheX, and CheC double mutants Glu13Ser + Glu112Ser (CheC dmE) or Asn16Ser + Asn115Ser (CheC dmN). Only CheY dephosphorylates CheA (lane 2). Both CheX (lane 10) and CheC (lane 6) reduce the amount of CheY-P, although CheX has much greater activity as no CheY-P remains in its presence. CheD activates CheC (lane 12) to roughly the same level as CheX (lane 10). CheC dmE and CheC dmN do not noticeably dephosphorylate CheY (lanes 7 and 8); however, CheD partially rescues the activity of dmE (lane 13), but not dmN (lane 14).
(C) Effects of CheC mutants on CheY-P in the presence of CheD. Bands corresponding to CheY-P after transfer from autophosphorylated CheA (CheA-^{32}P). Lanes 1–7 are controls as designated; lanes 8–13 are CheA+CheY+CheD+CheC mutants: Glu13Ser, Glu112Ser, Glu13Ser/Glu112Ser, Asn16Ser, Asn115Ser, and Asn16Ser/Asn115Ser, respectively. Coomassie-stained SDS-PAGE gel showing that the concentrations of the CheC mutants are equivalent.

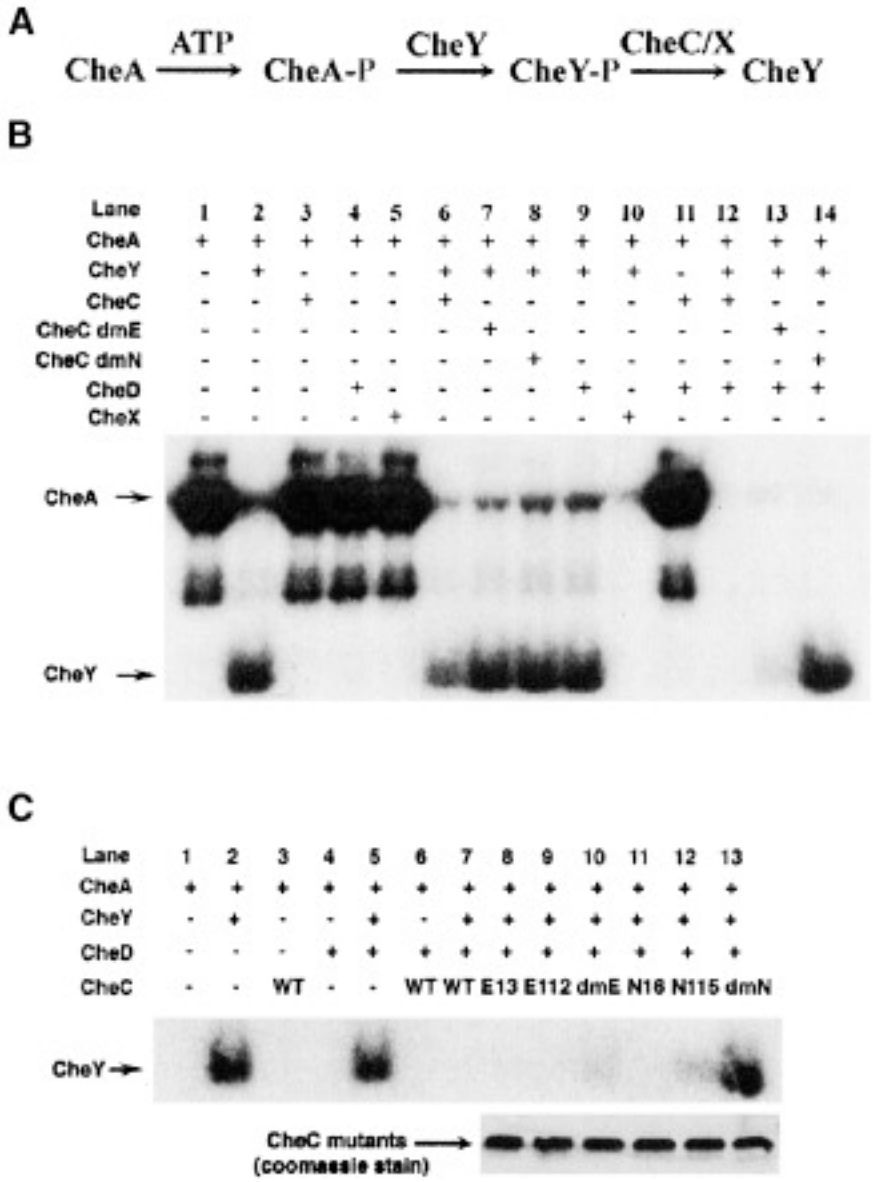
A
CheA
ATP
CheA-P
CheY
CheY-P
CheC/X
CheY
B
Lane 1 2 3 4 5 6 7 8 9 10 11 12 13 14
CheA + + + + + + + + + + + + + +
CheY - + - - - + + + + + - + + +
CheC - - + - - + - - - - + + - -
CheC dmE - - - - - - + - - - - - + -
CheC dmN - - - - - - - + - - - - - +
CheD - - - + - - - - + - + + + +
CheX - - - - + - - - - + - - - -
CheA
CheY
C
Lane 1 2 3 4 5 6 7 8 9 10 11 12 13
CheA + + + + + + + + + + + + +
CheY - + - - + - + + + + + + +
CheD - - - + + + + + + + + + +
CheC - - WT - - WT WT E13 E112 dmE N16 N115 dmN
CheY
CheC mutants
(coomassie stain)

Each conserved residue pair, Glu13/Asn16 or Glu112/Asn115, likely participates directly in CheY dephosphorylation, with the Asn residues being more critical for activity. Although the two centers reside on the same face of CheC they are far enough separated to each form distinct binding sites for CheY-P. In the presence of CheD, only the Asn16/Asn115 CheC double mutant increases CheY-P levels to those seen in the absence of CheC, whereas any one of the single mutants, with CheD, significantly reduces CheY-P levels. Thus, CheC appears to have two pseudosymmetric active sites, each marked by conserved Glu and Asn residues and each independently capable of dephosphorylating CheY. However, the mutagenesis studies also suggest that the Glu112/Asn115 active site is more active than the Glu13/Asn16 site (Figure C2), which is not surprising given the different overall residue compositions in these two regions.

REFERENCES

1. Parkinson, J.S. and E.C. Kofoid, *Communication modules in bacterial signaling proteins.* Annu Rev Genet, 1992. **26**: p. 71-112.
2. Park, S.Y., et al., *Structure and function of an unusual family of protein phosphatases: the bacterial chemotaxis proteins CheC and CheX.* Mol Cell, 2004. **16**(4): p. 563-74.